UC San Diego

UC San Diego Electronic Theses and Dissertations

Title

Phthalate Transfer and Enrichment in Artificial Sea Spray Aerosols

Permalink

https://escholarship.org/uc/item/6zj2v90m

ISBN

9798190945355

Author

Hedin, Molly Maevia

Publication Date

2026-09-16

Peer reviewed|Thesis/dissertation

eScholarship.org Powered by the California Digital Library
University of California

UNIVERSITY OF CALIFORNIA SAN DIEGO

Phthalate Transfer and Enrichment in Artificial Sea Spray Aerosols

A Thesis submitted in partial satisfaction of the requirements
for the degree Master of Science

in

Chemistry

by

Molly Maevia Hedin

Committee in charge:

Professor Jonathan Hall Slade Jr., Chair
Professor Stacey Brydges
Professor Vicki Helene Grassian

2026

Copyright

Molly Maevia Hedin, 2026

All rights reserved.

The Thesis of Molly Maevia Hedin is approved, and it is acceptable in quality and form for publication on microfilm and electronically.

University of California San Diego

2026

DEDICATION

To Owen and Elanor. My siblings, best friends, and two of my favorite soulmates. I could not have done this without you guys. Your love and laughter brings me peace amidst all the chaos. You are my rocks. I love you guys with my whole heart.

TABLE OF CONTENTS

LIST OF FIGURES

LIST OF TABLES

LIST OF ABBREVIATIONS

AER	Aerosol
BBP	Butyl benzyl Phthalate
CVD	cardiovascular disease
DBP	Dibutyl phthalate
DCM	Dichloromethane
DEHP	Di(ethylhexyl) phthalate/Bis(2-ethylhexyl) phthalate
DEHP-d_4	Deuterated di(ethylhexyl) phthalate
DMA	Differential mobility analyzer
DMP	Dimethyl phthalate
EF	Enrichment factor
EPA	Environmental protection agency
EU	European Union
GC/MS	Gas chromatography-mass spectrometry
IC	Ion chromatography
LOD	Limit of detection
MART	Marine aerosol reference tank
MCPC	Mixing condensation particle counter
MW	Molecular weight
PA	Palmitic acid
PAE	Phthalic acid ester
PFAAs	Perfluoroalkyl acids
PPL	Priority PolLutant

PVC	Polyvinyl chloride
QFF	Quartz fiber filter
RH	Relative humidity
SEMS	Scanning Electrical Mobility Spectrometer
SPE	Solid-phase extraction
SSA	Sea spray aerosols
SSML	Sea surface micro layer
SW	Sea water
ZAG	Zero particle air generator

ACKNOWLEDGEMENTS

I would like to first acknowledge Professor Jonathan Slade for his support, guidance, and patience as an advisor. I could not have asked for a more understanding mentor. His insight and encouragement have shaped both my research and professional development. I am very thankful for the opportunities he provided, his patience during challenging moments, and his confidence in my abilities. Beyond academia, I deeply appreciated the effort he made to get to know his students as people, fostering a lab environment that felt supportive, and genuine. I am very thankful to have been a part of the Slade lab.

I would also like to recognize my committee members Professor Stacey Brydges and Professor Vicki Grassian for their advice and guidance during my graduate education. I truly enjoyed working with Stacey, and the genuine connection we have.

I could not have completed this project without the constant support of the entire Slade lab. Thank you to Diana Tran, Kanuri Roundtree, Amelie Creekmore, Wen Zhang, Anna Vu, Cheryl Liu, Rachel Tseng, Xitlali Ventura, Maya Morris, and Lincoln Mehndiratta. I had so much fun working you all in the lab, and our gab sessions in the office. I would like to give a special thanks to Diana and Kanuri who provided so much guidance and support, I truly could not have completed this project without them. I am so grateful that I was able to be a part of this lovely group of people.

I would also like to thank amazing people outside of my academic career that provided constant support. Thank you to all my besties who kept me sane during my academic career. Thank you to my mom, Dr. Robin Keith, who constantly supports me through everything, I would not be who I am today without you. Thank you to my best friends and siblings Elanor and Owen, for all the support and love through this period of my life. Lastly, I want to thank Faith

Poutoa, my lovely girlfriend, who has been my biggest supporter throughout this experience. You have been there through the highs and lows and never wavered in support; I could not have done this without you.

Chapters 1 through 4, in part, coauthored with Slade, Jonathan H., is currently being prepared for submission for publication under the title, “Phthalate Transfer and Enrichment in Artificial Sea Spray Aerosols.” The thesis author is the primary researcher and author of this paper.

VITA

2024 Bachelor of Science in Chemistry with an emphasis in Biochemistry, San Diego State University

2026 Master of Science in Chemistry, University of California San Diego

2025 Teaching Assistant, University of California San Diego

2025 Research Assistant, University of California San Deigo

PRESENTATIONS

Phthalate Transfer and Enrichment in Artificial Sea Spray Aerosols — October 2025
Molly Hedin
UCSD (PI: Dr. Jonathan Slade)
American Association for Aerosol Research (AAAR) – Poster Presentation
In-Person Conference, Buffalo, New York

An ab initio investigation of the energetic properties of HC_3O radicals — March 2024
Molly Hedin
SDSU (PI: Dr. Andrew Cooksy)
San Diego State Student Symposium – Oral Presentation
In-Person Conference, California

FIELD OF STUDY

Major Field: Chemistry
Studies in Atmospheric Chemistry
Professor Slade

ABSTRACT OF THE THESIS

Phthalate Transfer and Enrichment in Artificial Sea Spray Aerosols

by

Molly Hedin

Master Science in Chemistry

University of California San Diego, 2026

Professor Jonathan Slade, Chair

Phthalates (Phthalic Acid Esters; PAEs) are widely used toxic plasticizers, and their contamination in oceans and air is widespread due to their leachability. Previous studies have detected PAEs in air and water in remote marine environments worldwide, suggesting their transfer from the ocean to the atmosphere. However, no prior work has quantified PAE enrichment in the ocean surface layer or in marine aerosols. Here, we investigate the transfer characteristics and enrichment factors (EFs) of three common PAEs: dimethyl phthalate (DMP),

dibutyl phthalate (DBP), and di(2-ethylhexyl) phthalate (DEHP), from artificial seawater to an artificial (i.e., palmitic acid) sea surface microlayer (SML) and in nascent sea spray aerosols (SSA). The relative extent of enrichment was found to depend on PAE hydrophobicity and volatility. DBP exhibited the highest EFs in both the artificial SML and nascent SSA compared to other phthalates. DBP EFs in the artificial SML from two independently prepared tanks were 34.3(±1.6) and 20(±3) when present alone and 21.1(±0.9) and 16(±3) when mixed with DMP and DEHP. DMP EFs in the artificial SML were 1.25(±0.10) and 5.45(±0.19) when alone and 1.47(±0.10) and 1.47(±0.07) when mixed. DBP was also significantly more enriched than DMP in nascent SSA, with EFs of 28800(±1300) and 16000(±7000) when alone, and 57400(±2500) and 35000(±8000) when mixed. DMP EFs in SSA were much lower, with values of 6(±12) and 450(±50) when alone and 3(±1) and 542(±24) when mixed. EFs for DEHP were inconclusive due to potential matrix effects, contamination, or degradation. Greater EFs were measured when particles with Dp > 300 nm were absent, suggesting a size dependence in phthalate enrichment in SSA, consistent with other contaminant enrichment studies. These results demonstrate, for the first time, that the sea surface layer and sea spray aerosols may strongly enrich certain PAEs, particularly DBP. This highlights the importance of the ocean surface in mediating the transfer of toxic phthalates from the ocean to the atmosphere.

Chapter 1: Introduction

1.1 Phthalate Contamination, Environmental, and Health Risks

Phthalic acid esters (PAEs) are widespread environmental contaminants used in a variety of products as plasticizers, with a base chemical structure shown in Fig. 1. First synthesized in the 1920s, the use of PAEs drastically increased with the production of polyvinyl chloride (PVC).[1,2] The production of PAEs continued to increase and by the 1970s, with over 1 billion pounds of PAEs being produced.[1] The uses had then diversified, PAEs were now being used in food and beverage packaging, personal care items, pharmaceuticals, laboratory equipment, and many other applications.[3–5] Table 1 from Mansuri et al. 2025 identifies just a few of the most common PAEs and their uses.[6] Since the 1970s, scientists have recognized the ubiquitous contamination of PAEs in the environment, but the impacts were unknown. [7]

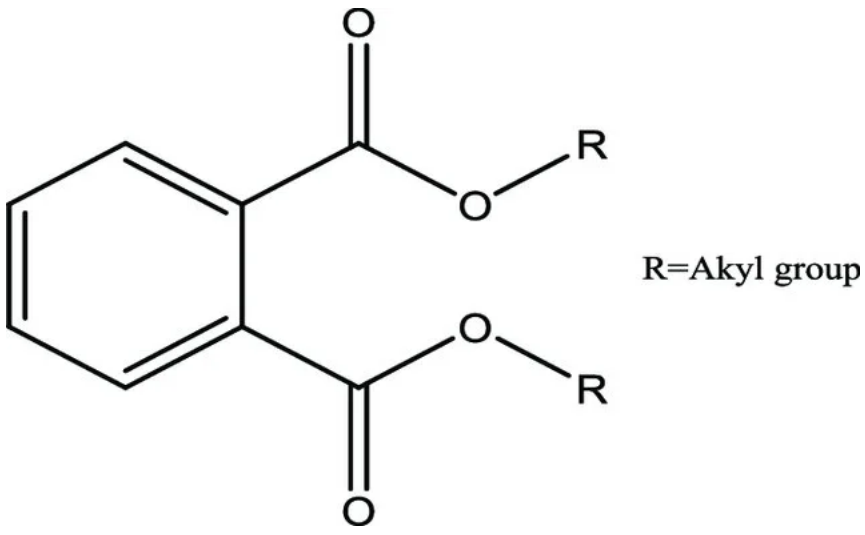

Figure 1. Base chemical structure of PAEs. [8]

Table 1. Common PAEs and their applications.[6]

Phthalate	Abbreviation	Formula	$\log K_{ow}$	Molar mass (g/mol)	Uses
Dimethyl phthalate	DMP	$C_{10}H_{10}O_4$	1.61	194.2	perfumes, hair sprays, lubricants, children's toys and medical devices
Diethyl phthalate	DEP	$C_{12}H_{14}O_4$	2.54	222.2	toothbrushes; automobile parts; tools; toys; food packaging; cosmetics; insecticides; aspirin
Di-n-butyl phthalate	DnBP	$C_{16}H_{22}O_4$	4.27	278.4	nail polishers; plasticizer; an additive to adhesives or printing inks
Diisobutyl phthalate	DIBP	$C_{16}H_{22}O_4$	4.27	278.4	plasticizer; adhesive
Butyl benzyl phthalate	BBP	$C_{19}H_{22}O_4$	4.70	312.4	plasticizer
Dihexyl phthalate	DHP	$C_{20}H_{30}O_4$	6.00	334.4	plastisols for automobile parts and dip-molded products
Diisoheptyl phthalate	DIHpP	$C_{22}H_{34}O_4$	6.87	362.5	plasticizer
Di(2-ethylhexyl) phthalate	DEHP	$C_{24}H_{40}O_4$	7.73	390.6	plasticizer
di-n-octly phthalate	DnOP	$C_{24}H_{38}O_4$	7.73	390.6	household items and building products; food applications
Diisononyl phthalate	DINP	$C_{26}H_{42}O_4$	8.60	418.6	plasticizer
Diisodecyl phthalate	DIDP	$C_{28}H_{46}O_4$	9.46	446.7	plasticizer
Diundecyl phthalate	DUP	$C_{30}H_{50}O_4$	10.33	447.7	electrical wire insulation and car interiors
Ditridecyl phthalate	DTDP	$C_{34}H_{58}O_4$	12.06	530.8	plasticizer for polyvinyl chloride in cable and high-temperature wire insulation

PAEs are not covalently bound to plastic products and readily leach into the environment.[9,10] PAEs are found throughout the oceans, with concentrations ranging from .04 ng/L to 168,000 ng/L in seawater and .002 ng/g to 35,000 ng/g in sediment.[11,12] Their ability to integrate into organisms, cross physical interfaces, and degrade, pose threats to the environment.[13–15] Redistribution of PAEs occurs through interface partitioning, including air/sea, air/particle, sea/sediment, and sea/organism.[16] Degradation of PAEs occurs via hydrolysis, photodegradation, and biotic processes.[10,17–20] The abiotic degradation half-lives of PAEs via hydrolysis range from >0.3 years for butyl benzyl phthalate (BBP) to 2000 years for (DEHP).[17] Atmospheric photooxidation half-lives range from as low as .02 days for DEHP to 93 days for DMP.[17,21]

Products of PAE degradation, such as phthalate monoesters, are associated with endocrine disruption, and health risks.[22]

Effects of PAEs in biological systems has been documented from fish to humans.[23–25] PAEs have been identified as endocrine disrupting and of having negative reproductive and health effects.[23,24,26] Human uptake of PAEs occur through consumption, skin contact, and inhalation.[26] Concentrations are tracked in humans through PAE metabolites, monoester phthalates. PAEs are metabolized in the body, and while shorter molecular weight (MW) PAEs are often excreted in urine, bulkier ones stay in the system longer and are subject to further oxidation.[26] Kolatorova et al. 2018 found that monoester phthalates were present in cord plasma of pregnant women, of which included metabolites of DBP, mono-butyl phthalate (MnBP), and DEHP mono-(2-ethylhexyl) phthalate (MEHP), mono-(2- ethyl-5-hydroxyhexyl) phthalate (5-OH-MEHP), and mono-(2-ethyl-5-oxohexyl) phthalate (5-oxo-MEHP).[27] Park et al. 2019 studied the reproductive dysfunction in zebrafish due to endocrine disruption by MEHP.[28] These studies found a correlation between PAE exposure and hormone disruption. Other health effects are known to be influenced by PAE exposure. Wen et al. 2022 investigated the impacts DEHP and its metabolites have on cardiovascular disease (CVD), finding that they can increase the severity of CVD.[29] The prevalence of PAE contamination in our environment, and adverse effects on human health via endocrine disruption requires a deeper examination into how we manage and regulate the ubiquitous existence of PAEs.

In the 1970s, when the contamination prevalence of PAEs was identified, the US Environmental Protection Agency (EPA) recognized six different PAEs as priority pollutants, three of which are included in this study: DMP, DBP, and DEHP.[30] The recognition of PAEs as hazardous pollutants spans continents; Canada, Mexico, the European Union (EU), Australia, New

Zealand, India, Japan, and China all have regulations regarding PAEs.[6] While many countries focus on consumption limits, Australia, New Zealand, and the EU have environmental regulations, limiting the concentrations of PAEs in freshwater ecosystems.[6,9] Despite the recognition of the dire effects of PAEs, little action has been taken in tightening regulations or finding a solution to the contamination. Dated December 31, 2025, the EPA announced an intent on regulating the use of five PAEs: butyl benzyl phthalate (BBP), dibutyl phthalate (DBP), dicyclohexyl phthalate (DCHP), diethylhexyl phthalate (DEHP), and diisobutyl Phthalate (DIBP).[31] The need for stricter regulations on PAE production is imperative to the health of the environment and its inhabitance.

The contamination of PAEs has integrated seamlessly into the environment, spanning the biosphere, lithosphere, and atmosphere.[32,33] The ability and ease to cross physical interfaces makes PAEs highly susceptible to contamination spread.[16] Benson and Fred-Ahmadu 2020 sampled sediment from the Gulf of Guinea, finding there to be a concentrations of PAEs as high as 164.09 mg/kg dw, of which was largely dominated by DEHP, DBP, and DMP.[34] Xie et al. 2007 found an air-sea exchange of phthalates occurring in the Arctic, where concentrations of DEHP in the ocean reached 3330 pg/L and 735 pg/m^3 in the particle phase in air.[15] Another account of air-sea exchange of PAEs was reported in Mi et al. 2023. They found that concentrations reached 0.17 ng/L in sea water and 0.072 ng/m3 in the particle phase for DEHP.[13] In marine ecosystems, PAEs can transfer into the air via particulate phases, such as sea spray aerosols (SSA). Physical mechanism of wave breaking, and bubble bursting likely promote this transfer of PAEs from the ocean into the atmosphere.

1.2 Sea Spray Aerosol Formation

Nascent SSA are produced via wave breaking and bubble bursting mechanisms (Fig. 2.)[35–38] When a wave breaks, it entraps and pushes pockets of air underneath the surface. These then rise to the surface as bubbles; film droplets are produced when the bubble ruptures, followed by jet droplets when the bubble cavity collapses.[38] A third SSA type, spume, is produced from droplets emitted from the crest of breaking waves.[38,39] SSA range in radii from 10 nm to millimeters, and are the largest source of atmospheric particles by mass.[38] The chemical composition of SSA depends greatly on the size of the particle, and sea surface microlayer components[36,37,40]

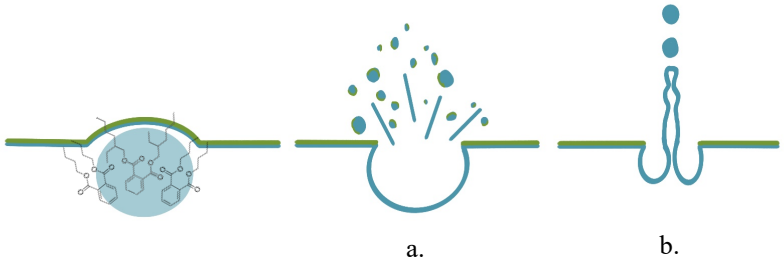

Figure 2. Bubble breaking mechanism, producing SSA. a. Film droplets, creating smaller aerosols with higher concentrations of surface contaminates. b. Jet droplet, producing larger aerosols containing primarily bulk sea matrix. DBP is shown as a representation of the orientation of molecules in bubbles.

Surface residing molecules, including surfactants and other weakly soluble compounds, interacting with the sea sea-surface micro layer (SSML) are able to transfer at the air-sea interface of bubbles.[36] Enrichment of surfactants in SSA is dependent on the absorption of molecules on to the bubble on its path to the surface.[41] Bubbles entrapped beneath the ocean's surface not only facilitate transfer of surfactants to the atmosphere, but are also key in transporting surface active molecules to the SSML.[42] Bubble scavenging is essential to the facilitation of surfactants to the SSML, and SSML reformation after a wave break. Composition of the SSML is directly related to the composition of SSA. Highly surfactant enriched SSA are

formed from film droplets, when the bubble reaches the surface and the bulk water is able to drain off.[42] Cochran et al. 2016, identified a key role of surface active molecules and the transfer in film droplets. This results in organic carbon compounds becoming more enriched in smaller submicron particles produced from film droplets.[37,43–45] Larger droplets in the super micron range are impacted more by water soluble components emitted in the jet (i.e., Na^+, K^+, Mg^{2+}, Ca^{2+}, and Cl^-).[37] Specific chemical properties of a species can also affect transfer in SSA. The octanol-water partitioning coefficient, K_{ow}, governs the ability of molecules to integrate in the SSML. Parameters such as the air absorption, and aqueous absorption coefficients will predict the molecules entrainment in bubbles on the way to the ocean's surface.[46] Studies on the SSML and SSA have identified the enrichment of supramolecules such as viruses, to trace contaminants.[47–52] Liu et al. 2026, found an enrichment temperature dependance for Perfluoroalkyl acids (PFAAs) in SSA. Size-dependent SSA composition has been noted in several studies, and these findings are a key aspect in understanding the effects SSA has on human health, and the environment.[44,53] Although this study does not directly investigate the size dependance of PAE transfer, results are indicative of size selective transfer, further discussed in results and discussion, and future work.

Chapter 1, in part, coauthored with Slade, Jonathan H., is currently being prepared for submission under the title, "Phthalate Transfer and Enrichment in Artificial Sea Spray Aerosols." The thesis author is the primary author of this chapter.

1.3 Thesis Objectives

This thesis aims to determine the enrichment of PAEs in the sea surface layer and in nascent SSA produced under controlled laboratory conditions. Matrices containing one phthalate species were studied and compared to a matrix with all the PAEs used in this study. An artificial seawater matrix containing a lipid layer with added quantities of PAEs in a Marine Aerosol Reference Tank (MART) was used to better mimic the conditions of SSA generation in the environment. Size distributions of the SSA are also analyzed using a Scanning Electrical Mobility Spectrometer (SEMS).

The scientific questions of this thesis address:

1. What are enrichment factors of phthalates, specifically DMP, DBP, and DEHP, in the sea surface layer and in nascent SSA, and do the physicochemical properties of PAEs influence enrichment?
2. Does the presence of different PAEs species affect the enrichment factor of a given PAE?
3. Does PAE enrichment in the sea surface layer correlate with enrichment in nascent SSA?

Chapter 2: Methods and Instrumentation

This section describes the experimental procedures, theory, and chemicals employed to study the EF of select PAEs in artificial sea surface water and nascent SSA. The PAEs selected for this study were DMP (≥99.5% purity), (DBP; (≥ 98% purity), and DEHP (≥ 98% purity), structures shown in Fig. 3. The deuterated internal standard was DEHP-d_4 (≥ 99% purity). The standards were PESTANAL® analytical standards purchased from Sigma Aldrich (St. Louis, MO). Stock and

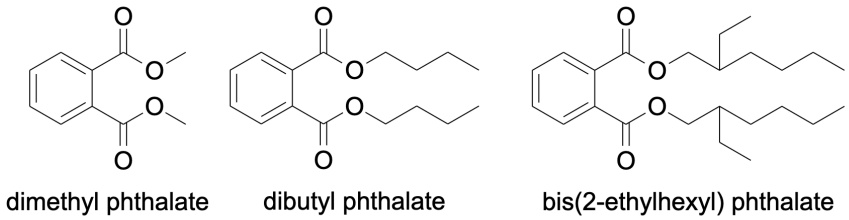

Figure 3. Chemical structures of Dimethyl phthalate (DMP, MW=194.184), Dibutyl phthalate (DBP, MW=278.344), and Bis(2-ethylhexyl) phthalate (DEHP, MW=390.556).

working solutions were prepared and diluted in dichloromethane (DCM; submicron filtered, high-performance liquid chromatography (HPLC) grade, sourced from Fisher Chemical (Pittsburgh, PA)). Other solvents used were acetone (submicron filtered) and methanol (0.2 micron filtered), both high-performance liquid chromatography (HPLC) grade, sourced from Fisher Chemical (Pittsburgh, PA). The artificial seawater matrix made to resemble environmental conditions was comprised of Milli-Q water, Biopak® Polisher sourced from Sigma Aldrich (St. Louis, MO), a reef sea salt mixture (Instant Ocean; SpectrumBrands, Blacksburg, VA), and palmitic acid ($C_{16}H_{32}O_2$), ≥95% purity, sourced from Sigma Aldrich (St. Louis, MO). To collect SSA, Whatman 90mm quarts microfiber filters (QFF), purchased from

Agilent (Santa Clara, CA), were used, then stored in VWR®, Sterile Sample Bags purchased from (Avantor). SSA size distributions were measured using a scanning electrical mobility Spectrometer (SEMS). Figure 4. shows the experimental setup. PAE analysis used Bond Elut PPL (Priority PolLutant) solid-phase extraction (SPE) cartridges (200 mg, 125 µg, 3 mL), purchased from Agilent (Santa Clara, CA). All experimental glassware was borosilicate glass, washed with acetone and DCM, and combusted at 200°C for 24 hours. Vials used for gas chromatography (GC) were cleaned and processed in the same way. These cleaning procedures helped minimize PAE contamination.[4]

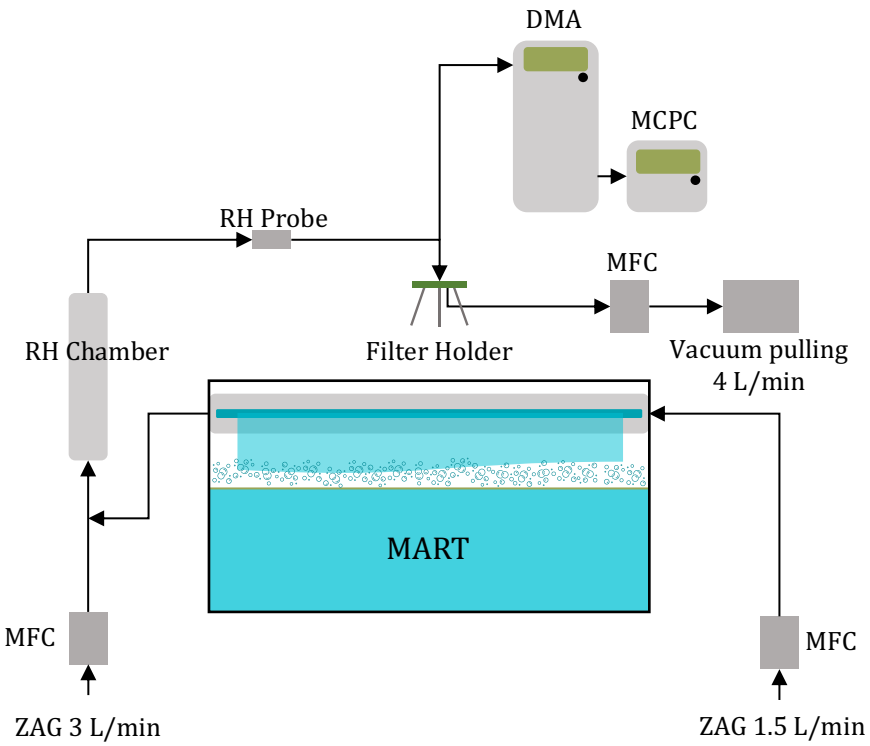

Figure 4. Experimental set up for PAE aerosol collection using a MART to mimic wave breaking and aerosol production. Collection occurred on QFF over 24 hours, SEMS and RH data were also collected simultaneously.

2.1 SSA Generation with a Marine Aerosol Reference Tank (MART)

The MART enabled production of nascent SSA in the lab. The MART was first described in Stokes et al. 2013, and has since been used in many studies.[35,54–57] The MART used in this study is a sealed rectangular plexiglass enclosure measuring 91 cm x 45 cm x 53 cm. An acrylic tube above the water line creates a plunging sheet of water, mimicking a wave break in the ocean. The water is continuously recirculated by an AMT commercial-duty pump. The intervals at which the sheet plunges can be set to a range of modes, affecting the concentration of SSA sampled. This study utilized intervals of 10s plunging, 10s off.

The MART generates SSA size distributions like those in natural conditions. However, it's noted that SSA size distributions may differ from the real marine atmospheric environment due to winds, differences in wave height, foam coverage, and biological activity. A constant supply of air from a Sabio model 1001 zero air source (zero air generator, ZAG), pressurizes the MART, preventing room air from entering the tank. Utilizing different air flows manipulates the relative humidity (RH) of the collected SSA, which can modify particle size due to changes in the equilibrium water content in the particles. This study flowed 1.5 L/min through the MART, controlled by an Alicat Mass Flow Controller (MFC), and was diluted by 3 L/min of dry ZAG air in a stainless-steel mixing chamber until the RH was constant. The RH and temperature of the air samples were continuously measured during aerosol collection using a Vaisala RH and T probe, which averaged 61(±6) % and 24(±0.8) °C, respectively. The RH was sampled after dilution from the ZAG, the RH in environmental conditions would be higher. It is likely that some evaporation of water from the aerosol after dilution with dry air reduced the particle size after the

aerosols left the MART. However, since the RH was consistently around 61%, the particles remained in a deliquesced liquid state during sampling.

In this study, conditions in the MART were used to mimic conditions in the environment. The MART was filled with 141 L of Milli-Q water (18 MΩ cm resistivity), then brought to an average salinity of 35.01 g/L with artificial reef salt. Details on the matrix for each experiment are presented in Table 2. Palmitic acid was dissolved in acetone and applied to the surface of the artificial sea matrix at concentrations of 35 μM, or .0089 g/L, as a chemical proxy of the sea surface microlayer.[43,58] While other studies use chloroform to dissolve PA, the solubility increases in acetone, allowing a more even application to the surface.[58] Continuous sampling of aerosols, RH, temperature, and size distributions occurred during the extent of each experiment running 24 hrs.

Table 2. Experimental components of the artificial sea matrix, including amount of water, salt, PA, and PAEs. The PAE concentration units are grams of PAE per gram of seawater.

Experiment	Volume (L)	Salt (g/L)	PA (g/L)	DMP (g/g)	DBP (g/g)	DEHP (g/g)
1	138.83 ± .02	35.04 ± .99	0.0089 ± .0002	$3.36E^{-07}$ ± $7.03E^{-10}$	0	0
2	142.59 ± .02	35.00 ± .99	0.0089 ± .0002	0	$3.21E^{-07}$ ± $6.84E^{-10}$	0
3	141.75 ± .02	35.00 ± .99	0.0089 ± .0002	0	0	$3.31E^{-07}$ ± $6.88E^{-10}$
4	142.31 ± .02	35.01 ± .99	0.0089 ± .0002	$3.80E^{-07}$ ± $6.86E^{-10}$	$4.04E^{-07}$ ± $6.86E^{-10}$	$3.17E^{-07}$ ± $6.86E^{-10}$
5	140.50 ± .02	35.00 ± .99	0.0089 ± .0002	0	0	$3.16E^{-07}$ ± $6.94E^{-10}$
6	142.73 ± .02	35.00 ± .99	0.0089 ± .0002	3.78E-07 ± $6.84E^{-10}$	0	0
7	143.42 ± .02	35.00 ± .99	0.0089 ± .0002	0	3.07E-07 ± $6.80E^{-10}$	0
8	142.87 ± .02	35.00 ± .99	0.0089 ± .0002	2.69E-07 ± $6.83E^{-10}$	2.60E-07 ± $6.83E^{-10}$	2.81E-07 ± $6.83E^{-10}$

2.2 Aerosol Size Distribution Measurement

This study utilized a Brechtel 2100 Scanning Electrical Mobility Spectrometer (SEMS), comprised of a Differential Mobility Analyzer (DMA) column in tandem with a model 1720 Mixing-based Condensation Particle Counter (MCPC), shown in Fig. 5. The SEMS measures submicron (≤1 μm) aerosol size distributions. The scanning mode was utilized for this study, collecting a size distribution between 5 nm and 850 nm across 100 bins at an 80 s sampling rate for 24 hours. Sections 2.2.1 and 2.2.2 further discuss the theory of the DMA and MCPC.

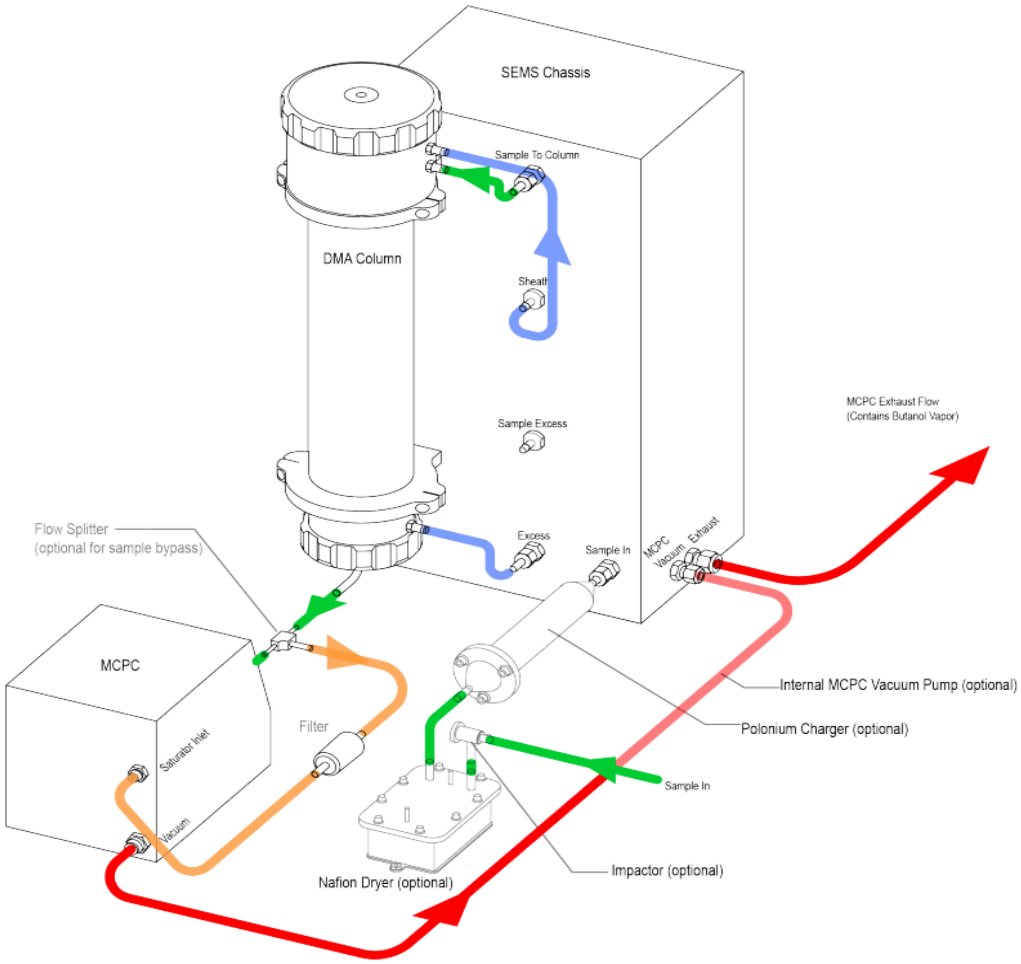

Figure 5. Schematic of Brechtel 2100 SEMS, including a DMA column, and MCPC. [50] This diagram shows an optional Nafion dryer, which was not used in this study.

2.2.1 DMA

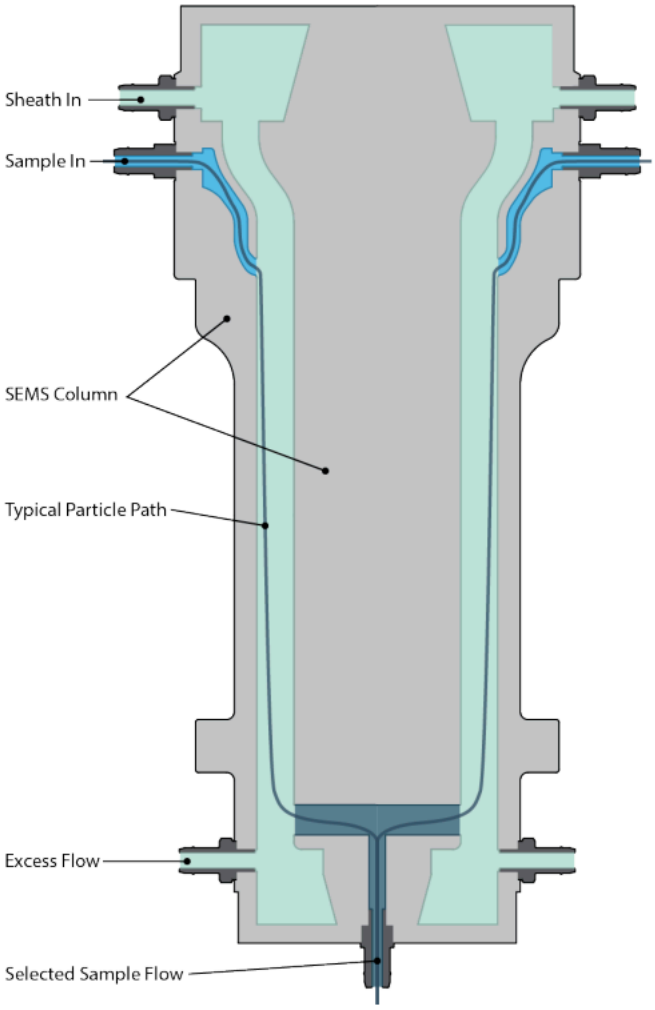

Figure 6. Cross section diagram of DMA.[50]

The differential mobility analyzer (DMA, Fig. 6) size segregates charged particles according to their electrical mobility in an applied electrical field. At the instrument inlet, aerosols are charge neutralized (i.e., given an equal number of positive and negative charges) by passing the aerosol sample over Polonium-210 strips. The particles enter the DMA at a flow rate

of 0.36 LPM, then mixed with a sheath flow set to 3.6 LPM. Inside the DMA is an unipolarly-charged stainless steel rod. The oppositely charged particles are attracted to the rod. Particles are either recirculated through the DMA, deposited to the rod, or exit the DMA. This is controlled by the rod's set voltage. Smaller particles with less momentum exit the DMA at low voltages while larger particles are recirculated. As the DMA voltage increases, larger particles exit the DMA while smaller particles deposit to the rod. By scanning the voltage to higher voltages, larger particles exit the DMA where they are counted by the condensation particle counter (CPC), described in more detail in section 2.2.2. The electrical mobility (Z) is related to particle mobility diameter (d_m) through the following equation:

Equation 1. $$Z(p,\ d_m) = \frac{neK_BTC_c(d_m)}{3\pi n_g d_m}$$

Here, n is the number of elementary charges, K_B is Boltzmann's constant, T is temperature, C_c is the Cunningham slip correction, and n_g is the dynamic air viscosity. Factors that can affect the accuracy of particle transmission through the DMA include multiple charges on the particles. The difference in the targeted mobility and actual mobility depends on the charge state at a given diameter. The particles are assumed to adopt a Boltzmann distribution of positive and negative charges centered around neutral (zero charge, when the number of positive and negative charges are equal) to as many as three or more charges in either the positive or negative direction. For such cases, large particles with a greater amount of charge may be attracted to the central rod at lower voltages than anticipated, leading to erroneously detected smaller particles. We apply the manufacturer-provided multiple-charge correction algorithm to eliminate these issues.

2.2.2 CPC

The particles exiting the DMA are then counted optically by the condensation particle counter (CPC). The Brechtel mixing CPC (MCPC) employs butanol vapor to saturate the aerosol sample with butanol. The particles grow due to butanol condensation to sizes detectable with an infrared laser detector. The count rate is 180 milliseconds dependent on the transit time through the detector. Here, particle number concentrations can be detected accurately between 0 and 100,000 cm^{-3} with an uncertainty of ±8% at 100,000 cm^{-3}. Particle losses in the sample tubing from the inlet of the DMA to the CPC are accounted for automatically using a diffusion correction algorithm. For all experiments, the diffusion correction was applied to correct for losses to the wall due to diffusion.

2.3 PAE and Na^+ Sampling and Extractions

2.3.1 SSA Sampling and Extraction

Aerosols generated in the MART were collected for 24 hours continuously onto QFFs (90 mm in diameter; 1 μm pore size) housed in a Millipore stainless steel filter holder. The filters were kept in an oven at 200°C for 24 hours prior to sampling. An external vacuum pump was attached behind the filter holder and sampled at a rate of 4 L/min measured by a Sairgo MF5700 Mass Flow Meter (MFM). This flow rate and collection time were chosen to ensure sufficient PAE aerosol mass had deposited onto the filters for analysis.

Filter extractions were performed using a modified method from Cooper et al. 2025.[46] The filter was cut using metal scissors and tweezers, first cleaned with acetone and methanol. Three fourths of the filter was used for PAE analysis, while a quarter was used for Na^+ analysis. For PAE extraction, the filter was submerged in glass scintillation vials with DCM and sonicated for 1 hour in a Branson Bransonic® Mechanical Bath 3800. The sonicated solution was then filtered using a Hamilton 50 mL glass syringe, and Acrodisc® 13mm .45μm Supor® filters. The filtered solution was aliquoted into GC vials, spiked with DEHP-d_4, and analyzed on the day of extraction or stored at -20°C until the next day.

Na^+ filter extractions were performed on the quarter portion of the filter not used for PAE analysis. The filters were placed in plastic vials, submerged in Milli-Q water, and then sonicated for 30 min. The sonicated solution was then syringe-filtered, and aliquots were placed in IC vials for processing on the day of extraction.

2.3.2 Sea Surface Layer Sampling and Extraction

Sea surface layer samples were collected using a 28 x 20 cm glass plate, a glass funnel, and a rubber squeegee.[38,59] It was noted that the rate of plate removal from the MART to collect the surface layer sample was faster than desired, resulting in larger sample volumes than anticipated. The rate of removal was 5 cm s^{-1}. However, the plate was not allowed to drain for 20 s, as described by Cunliffe and Wurl 2014.[59] The potential effects of the larger sample volume on the reported PAE concentrations from the surface layer are explored in section 3.1.3 Sea Surface Layer Analysis.

Sea surface layer samples were extracted via solid phase extraction (SPE), using the Bond Elut PPL SPE cartridges and a Restek Visiprep vacuum manifold.[33,60,61] Samples were frozen on the day of collection and thawed on the day of extraction. The cartridges were successively cleaned three times with 3 mL of acetone, then 3 mL of DCM. Conditioning of the cartridges used the same solvents; they were washed with 3 mL of acetone, 3 mL of DCM, and 3 mL of Milli-Q water. The total sample size for SSML was less than 5g; the sample was thus poured directly into the PPL tube, and filtered through the cartridges under vacuum at a rate of 1-2 drops per second.[60] After filtration, the cartridges were rinsed with 3 mL of Milli-Q water to remove excess salt and dried under vacuum for 30 minutes.[60] PAEs retained were eluted twice with 3 mL of DCM into pre-combusted glass vials. Paluselli et al. 2018, from which this extraction method was derived, obtained recovery rates for DCM being used as both the elution fractions.[60] DMP had a 100% recovery rate, DBP with 85%, and DEHP with 87%. 1 g aliquots were then transferred to GC vials, spiked with DEHP-d_4, and analyzed the day of the extraction or placed in a -20°C freezer until the next day.

For Na^+ extraction, 5 mg samples were aliquoted by a PU07709 Thermo scientific pipette into 10 mL conical vials and filled with 5-10 g of Milli-Q water. The samples were then sonicated for 30 min to ensure a homogenous solution. Aliquots were then placed in ion chromatography (IC) vials and analyzed on the same day.

2.3.3 Bulk SW Sampling and Extraction

Bulk artificial SW was collected via a side port on the MART into cleaned and pre-combusted 1 L amber glass bottles. Na^+ samples were taken from the same port into 10 mL conical vials. PAE extraction was performed using the same procedure as extraction of the sea surface layer samples, described above, with slight modifications. The 1 L samples were filtered through the cartridges through SPE tubing adaptors, under vacuum at a rate of 1-2 drops per second.[60] After, the cartridges were rinsed with 3 mL of Milli-Q water to remove excess salt and dried under vacuum for 1 hour.[60] The PAE elution and GS/MS prep is as described in the procedure for sea surface layer sampling.

10 mL samples of bulk SW were diluted in a series of dilutions for analysis. 5 mg samples were aliquoted from the sample by a PU07709 Thermo scientific pipette into 10 mL conical vials. The procedure then follows the exact steps of the sea surface layer extraction and IC prep.

2.4 GC/MS

Gas chromatography-mass spectrometry is a widely used analytical tool for analyzing PAEs.[4,13,20,60,62] Extracted sample analysis was performed on a Thermo Trace 1300 GC coupled with a TSQ 8000 Evo triple quadrupole (TSQ) mass spectrometer (GC/MS), using EI ionization (70 eV). An Agilent HP-5MS capillary column (30 m x 0.25 mm, 0.25 μm film thickness), with a GC oven temperature ramp starting at 50°C for 5 minutes, and then up to 250°C at 25°C/min, with a final isothermal hold for 5 min, was used for separation. Helium was used as a carrier gas at a flow rate of 1 L/min. The samples (1 μL) were injected using an automatic spitless sampler. Data was analyzed on Xcalibur, and PAE concentrations were quantified using external calibration curves. Calibrations and mass spectra are discussed in section 3.1.1 and 3.1.2.

2.5 IC

Extracted Na^+ samples were analyzed using a Thermo Dionex ICS-2000 IEC-CD. The instrument ran on positive mode using 18 mM methanesulfonic acid (MSA) as the solvent. An isocratic flow of .25 mL/min ran 20 min, with the suppressor set at 14 mA. 25 μL samples were injected into the loop and eluted in Thermo Dionex IonPac CS12A (2 x 250 mm) column, with a Thermo Dionex IonPac CG12A (2 x 50 mm) guard. Data was analyzed on Chromeleon, and concentrations were quantified using external calibrations. Calibrations are discussed in section 3.2.

2.6 Enrichment Factor Calculation

The EF values were calculated from Eq. 2.[63] Here, EF_X is a unitless value of chemical X. X_{AER}, X_{SML} and X_{SW} are concentrations in the aerosol (AER), sea surface layer (SML), and bulk seawater (SW) phases, respectively. These are normalized to the concentrations of Na^+, a seawater tracer, in the sample media, and then dividing the same ratio in bulk seawater. An EF>1.0 means that the PAE/Na^+ ratio is greater than in the bulk water, indicating PAE is enriched with respect to Na^+ in that sample. An EF=1.0 means the ratio of PAE/Na^+ is the same as in the bulk water, indicating no PAE enrichment. An EF<1.0 means PAE is enriched in the bulk water with respect to the sample and therefore depleted in the sample.

Equation 2.

$$EF_X = \frac{[X]_{aer} / [Na^+]_{aer}}{[X]_{SW} / [Na^+]_{SW}}$$

Chapter 2, in part, coauthored with Slade, Jonathan H., is currently being prepared for submission under the title, "Phthalate Transfer and Enrichment in Artificial Sea Spray Aerosols." The thesis author is the primary author of this chapter.

Chapter 3: Results and Discussion

3.1 PAE Detection and Analysis

3.1.1 Mass Spectra of PAEs

PAEs were detected and quantified from GC/MS data on Xcalibur. Specific *m/z* ratios were used as qualification and quantification peaks described in previous studies.[60,60,64–66] Yin et al. 2014 described the fragmentation pathway of common PAEs using GC/MS (Fig. 7). Although DBP and DEHP are described to have a similar fragmentation pathway, the mass spectra show different *m/z* abundances and retention times. Quantification and qualification peaks were chosen based on previous studies analyzing PAEs in the environment, listed in Table 3.[13,60,67] 149 was used as a quantifier peak for both DBP and DEHP, however they have different qualifier fragments, displayed in Figs. 8 and 9.

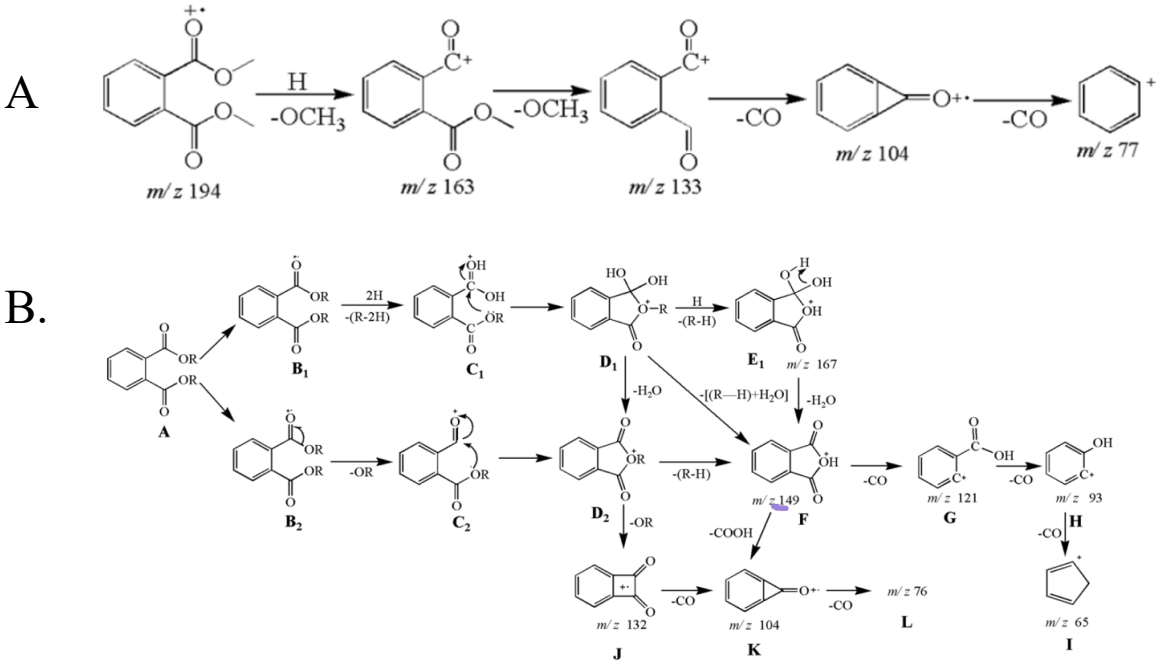

Figure 7. GC/MS fragmentation pathway of A. DMP, and B. DBP and DEHP. [56]

Table 3. Retention times, qualification, and quantification ions of PAEs by GC/MS.

xf	MW	Retention time	Quantification	Qualification
DMP	194.2	12.25	163	194, 135, 77
DBP	278.4	14.76	149	223, 205
DEHP	390.6	15.53	149	279, 167

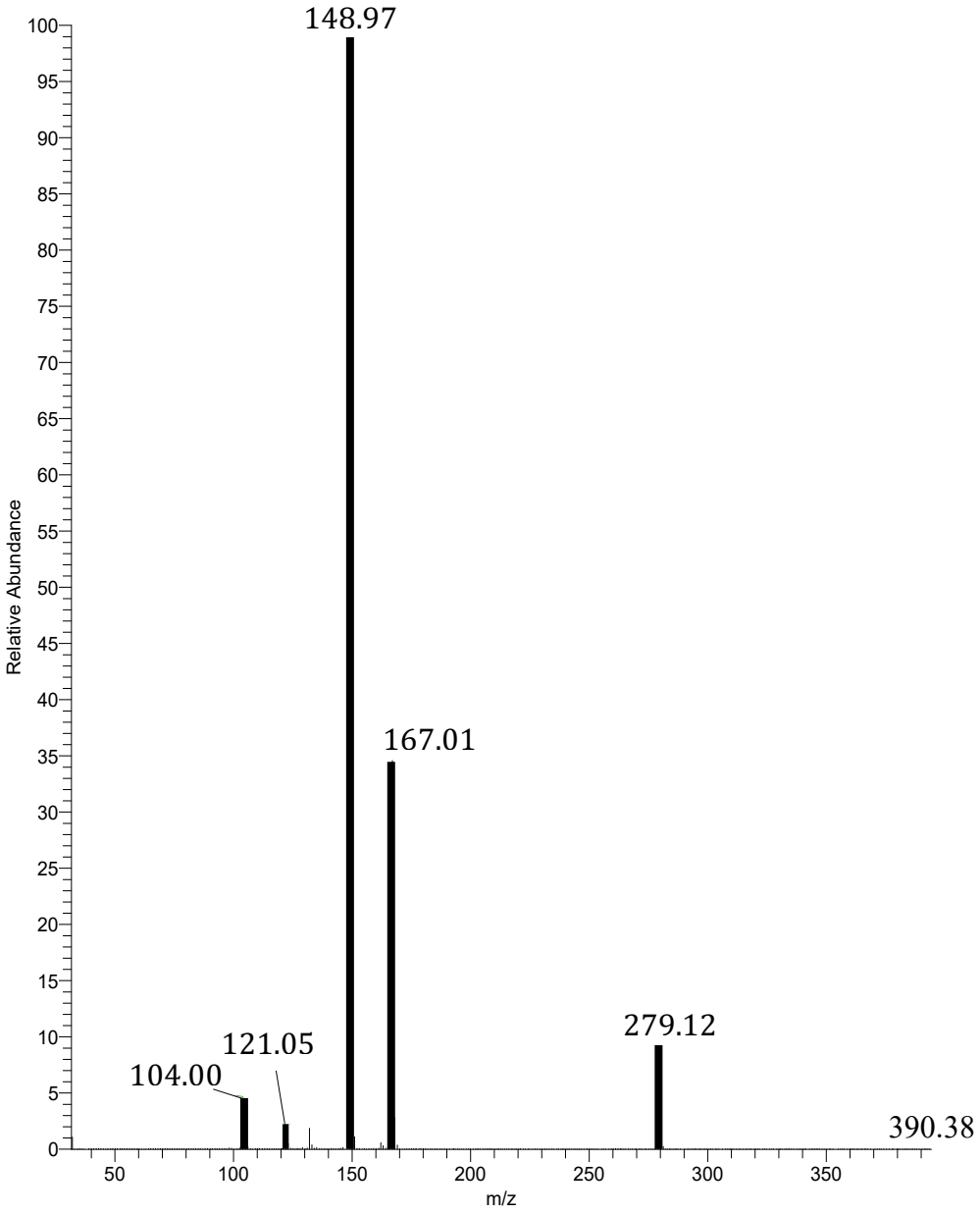

Figure 8. Mass spectra of DEHP

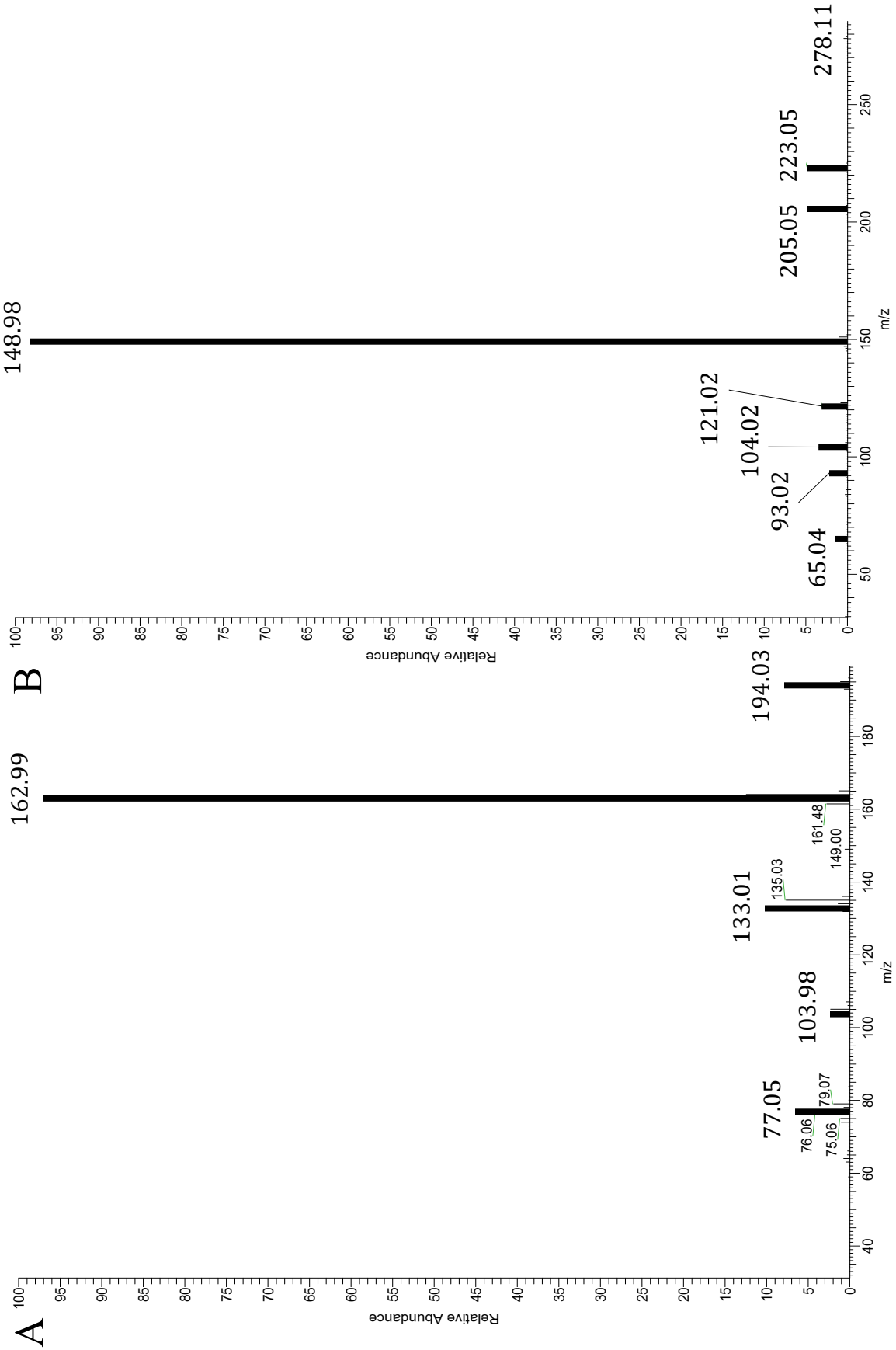

Figure 9. Mass spectra of a. DMP and b. DBP from signal in bulk sea water sample.

3.1.2 PAE Calibrations

External calibrations were performed on each PAE and used for quantification of PAE in the sample extracts. Both external calibration standards and the extracts were prepared in DCM. Because these calibrations were preformed using DCM, there is added uncertainty in the accuracy of calculating a samples concentration due to matrix differences. To minimize matrix effects, DEHP-d_4 was added to the samples as an internal standard. The calibration curves were linear across .5ng/g to 500µg/g, in the same range as the experimental data. Calibration curves for DMP, DBP, and DEHP are displayed in Figs. 10-12. Calibrations for DMP and DBP were run for the two data sets analyzed. One calibration curve was calculated for DEHP because the samples were run in immediacy. The limit of detections (LODs) of DMP, DBP, and DEHP are displayed in Table 4. The calibration curves used for the second round of DMP and DBP extractions were a higher range because of higher PAE concentration added to the MART.

Table 4. LODs of DMP, DBP, and DEHP. Values were calculated using calibration curves.

Calibration Curve	LOD (g/g)
DMP (25/07/22) - (25/08/23)	3.08×10^{-09}
DMP (25/11/18) - (25/12/23)	2.05×10^{-08}
DBP (25/07/25) - (25/08/23)	2.76×10^{-09}
DBP (25/11/18) - (25/12/23	1.06×10^{-07}
DEHP	1.46×10^{-08}

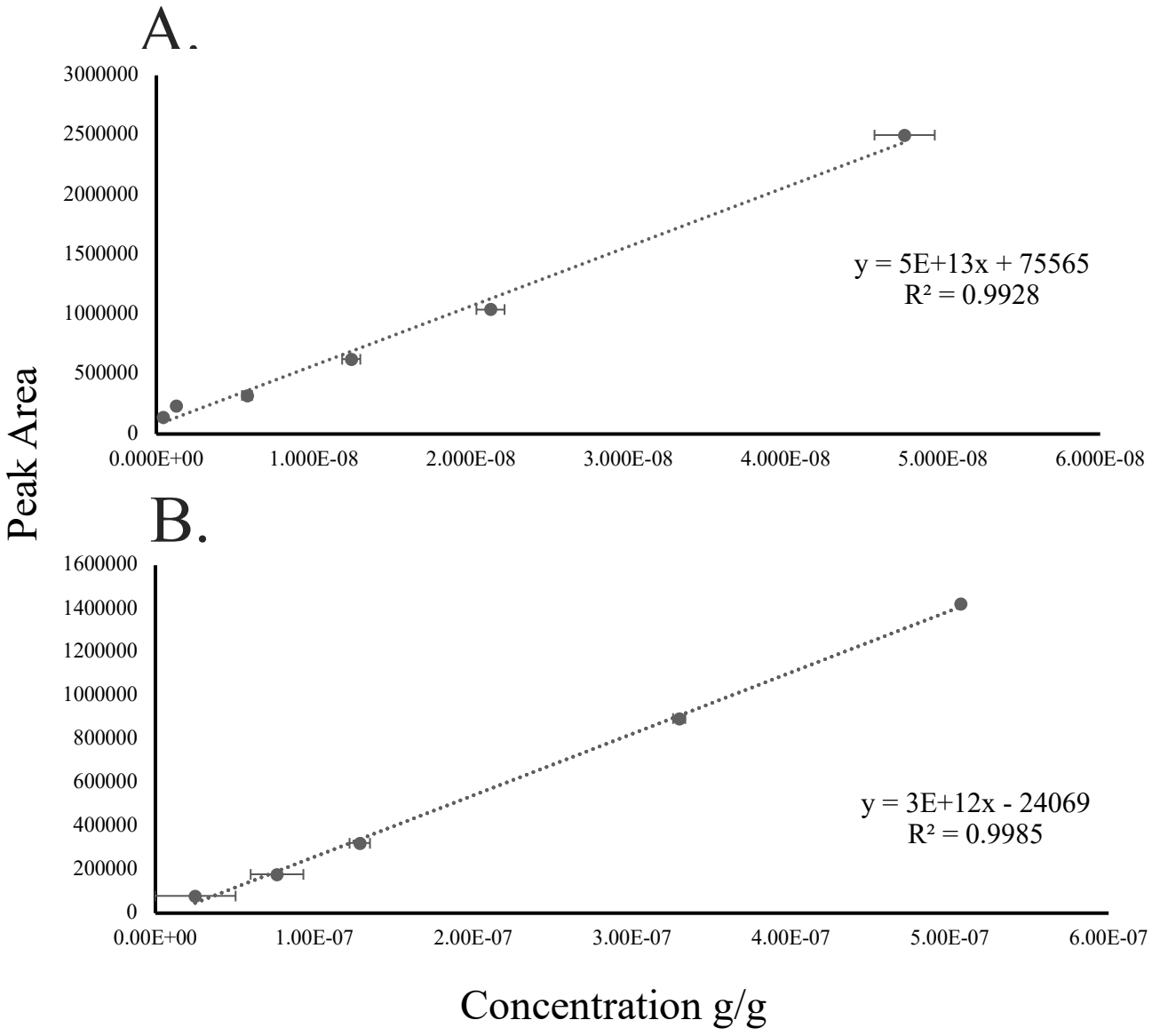

Figure 10. Calibration curves for DMP. Calibration A. was calculated with the first experiments (25/07/22) - (25/08/23), with a concentration range of $4.927x10^{-07}$ to $4.389x10^{-10}$ g/g. The slope is $4.97x10^{13}$ with an R^2 value of 0.9928. B. was calculated with the second set (25/11/18) - (25/12/23), with a concentration range of $2.50x10^{-08}$ to $5.07x10^{-07}$ g/g. The slope is $2.83x10^{12}$ with an R^2 value of 0.9985.

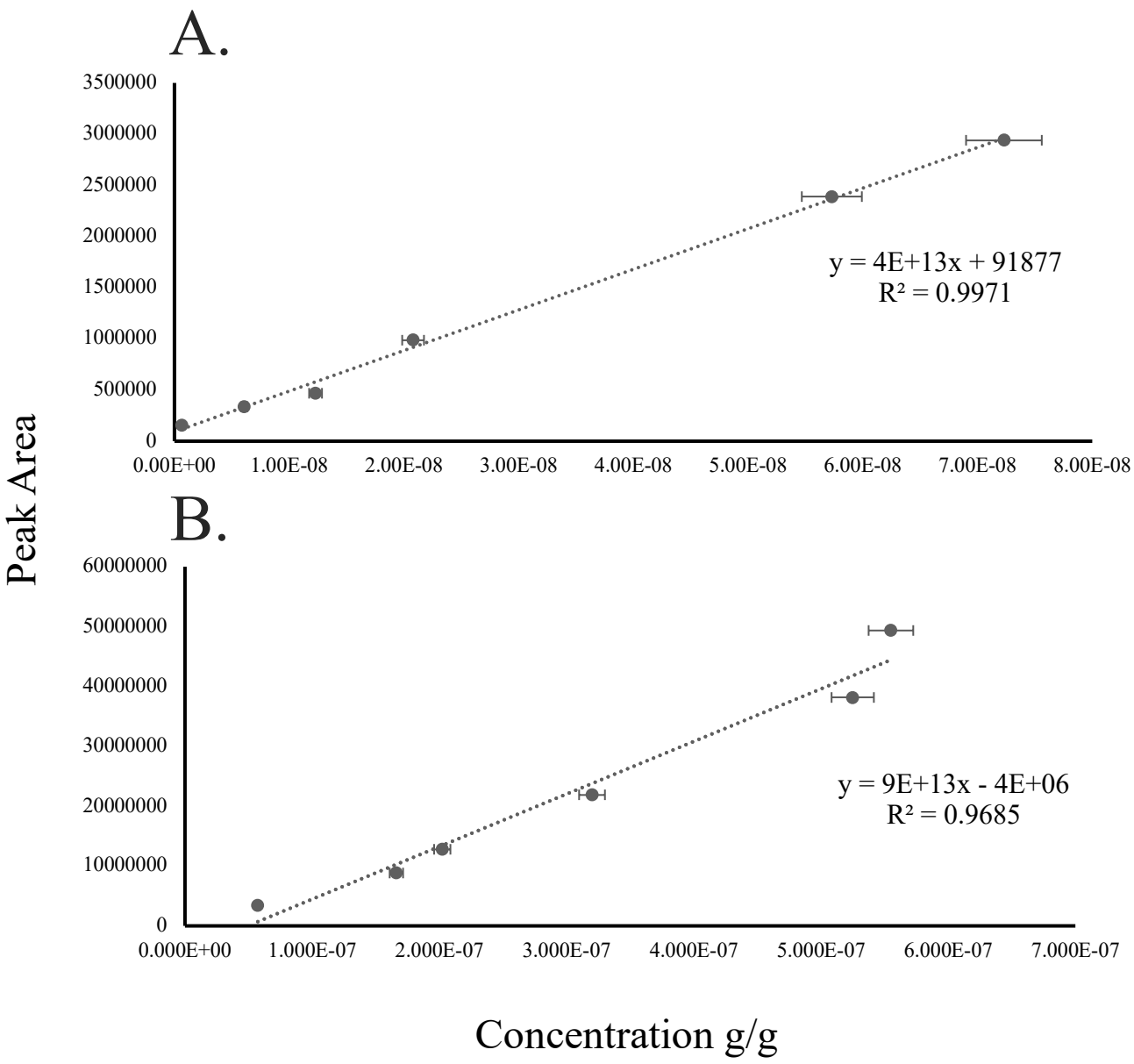

Figure 11. Calibration curves for DBP. Calibration A. was calculated with the first experiments (25/07/25) - (25/08/23), with a concentration range of $6.26x10^{-07}$ to $6.40x10^{-10}$ g/g. The slope is $3.96x10^{13}$ with an R^2 value of 0.9971. B. was calculated with the second set (25/11/20) - (25/12/13), with a concentration range of $5.550x10^{-07}$ to $5.727x10^{-08}$ g/g. The slope is $8.78x10^{13}$ with an R^2 value of 0.9685.

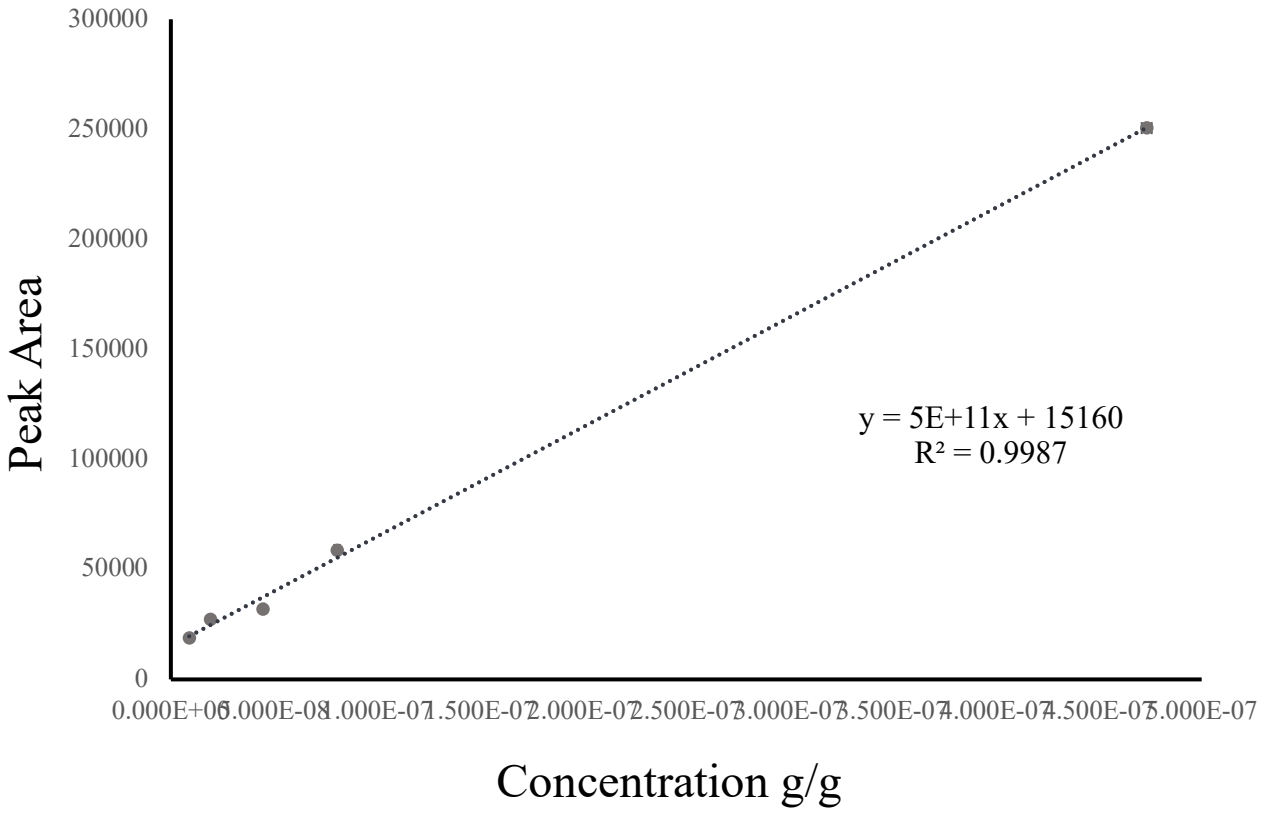

Figure 12. Calibration curves for DEHP, with a concentration range of 8.91×10^{-09} to 4.73×10^{-07} g/g. The slope is 4.98×10^{11} with an R^2 value of 0.9987.

3.1.3 Sea Surface Layer Analysis

The thickness of the artificial SSML, or sea surface layer, was calculated using Equation 3, described by Cunliffe and Wurl 2014.[59] Where V is the sample volume (cm^3), A is the immersed plate area, total of both sides (cm^2), N is the number of dips per sample, and h is the SSML thickness in μm.[59]

Equation 3. $$h = 10^4 \times {}^{V}/_{(A \times N)}$$

The average calculated sea surface layer thickness was 15(±2) μm, and values for each trial are displayed in Table 5. Wurl et al. 2017 sates that the SSML ranges from 1-1000μm depending on the collection method, where other studies find the thickness to lie around 50(±10) μm.[68–71] The values for this study are on the lower end of what was collected from environmental samples. This difference may be due to the artificial surface containing only one compound, whereas the real SSML contains thousands of compounds mixed with biological material that form extensive networks of colloidal material and hydrogels, contributing to a thicker, and more viscous SSML. The in-lab sampling may have also influenced on the thickness because of the state of the water. The ocean surface is in constant motion with no surrounding walls; here, however, the water was contained on all sides by plexiglass. It is likely that the cascading waterfall, when activated, disrupted the surface layer, pushing some of the surface components to the walls.

Table 5. SSML thickness in μm, calculated using Equation 3.[59]

Experiment	Sample Mass (g)	SSML thickness μm
DMP (25/07/22)	9.6607	15.7084
DBP (25/07/25)	10.3179	16.7770
ALL PAE (25/08/23)	10.8458	17.6354
DMP (25/11/18)	6.4236	13.9266
DBP (25/11/20)	6.0071	13.0236
ALL PAE (25/12/13)	6.6200	14.3522

3.2 Na^+ Detection and Calibration Curve

External calibration curves performed with IC were used to determine the concentrations of Na^+ in the collected samples. Concentrations for the curve ranged from $1.147x10^{-05}$ to $3.460x10^{-09}$ g/g (Fig.13). The calculated LOD was $3.82x10^{-8}$.

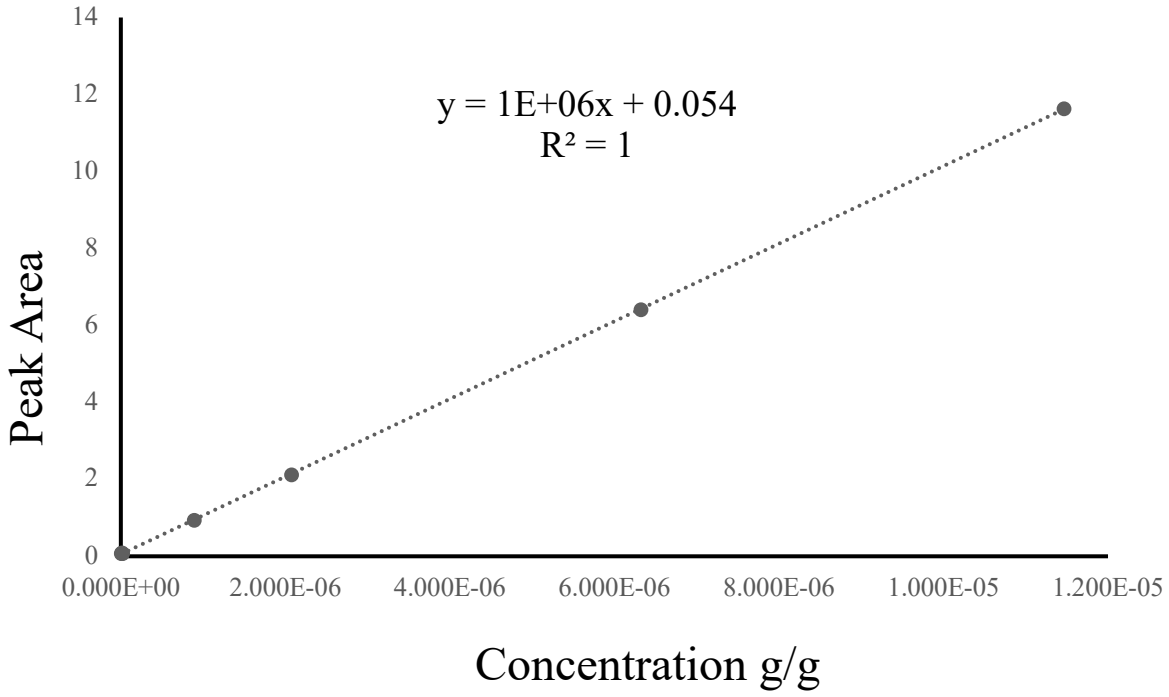

Figure 13. Na^+ calibration curve ranging from $1.147x10^{-05}$ to $3.460x10^{-09}$ g/g, with a slope of $1.01x10^6$ and an R^2 value of 1.

3.3 Enrichment Factors of PAEs in the sea surface layer and nascent SSA

We first examine the EFs, presented in Fig. 14 and Table 6, for DMP and DBP in the surface layer samples. High enrichment in the surface layer is indicative of the presence of more hydrophobic and surface-active species.[35] Two independent MART trials of each, DMP by itself, or DMP mixed with all other PAEs, were performed using similar starting concentrations on different dates in freshly made artificial seawater. The EF values for DMP by itself in the SML

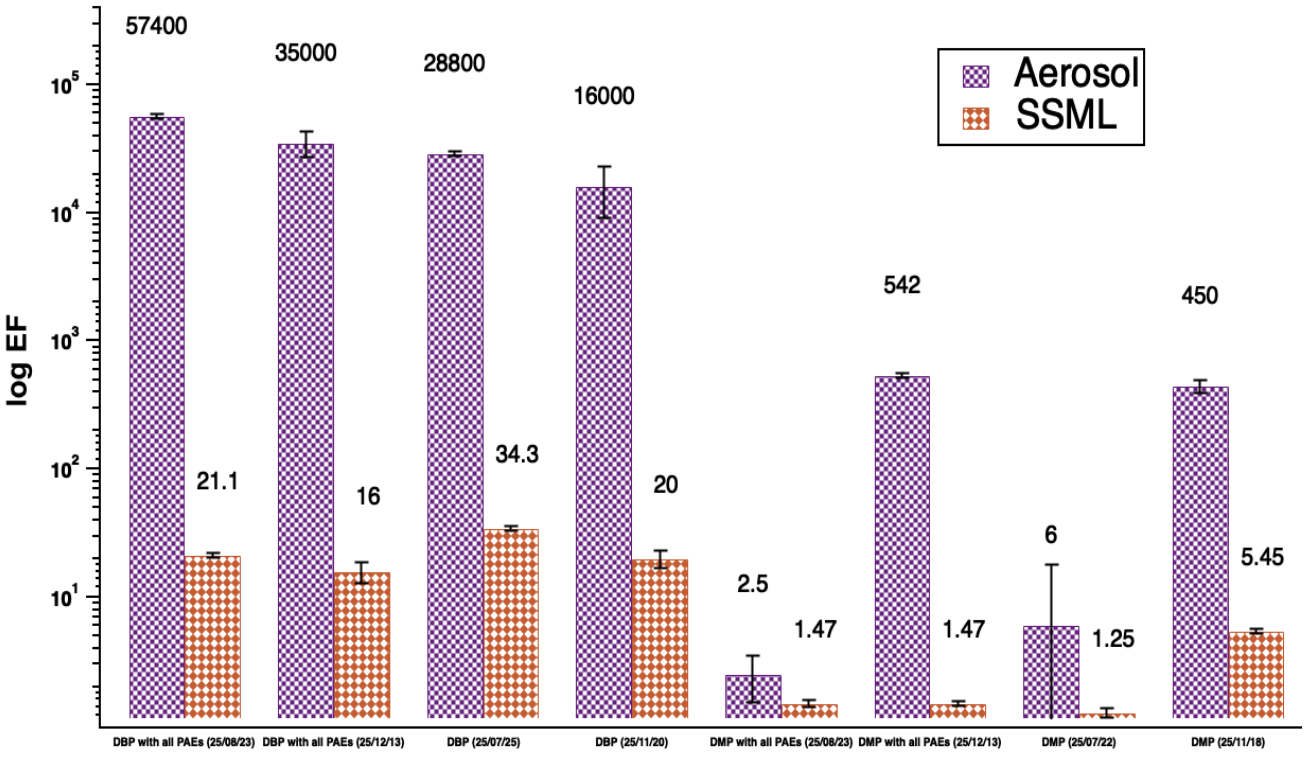

Figure 14. EF SSA and SSML values calculated using Equation 2.

were 1.25(±0.10) and 5.45(±0.19) for the two trials. The EF values for DMP mixed with other PAEs in the SML were 1.47(±0.10) and 1.5(±0.7), within the uncertainty and range of the EFs for DMP alone. Reasons for the greater SML enrichment in one of the trials of DMP alone are difficult to quantify, though enrichment in the SML can be affected by water temperature, the presence of dissolved ions and organic matter, and the stability of the SML.[42,68,72–74] These were

prepared and sampled in the same way between trials. However, it is possible that the SML was more stable and that more SML sample mass was collected in the higher enrichment trial. Conversely, DBP EFs in the SML were 34.3(±1.6) and 20(±3) when present by itself and 21.1(±0.9) and 16(±3) when mixed with other PAEs. None of these are significantly different from each other, though they are significantly more enriched in the SML than DMP.

Previous studies report varying EFs for different organic species in the SML, though none have reported on PAEs. In Trilla-Prieto et al., 2024, a series of organophosphate esters (flame retardants) were found to be relatively more concentrated in the SML compared to underlying waters in the Atlantic and Southern Oceans.[48] The EFs were reported as 5.84(±8.97) and 9.10(±9.48) for the Atlantic and Southern Oceans, respectively. EFs of polychlorinated biphenyls (PCB) and other organochlorine compounds in the SML were reported as ranging from 0.2 to 7.4 in offshore waters in Barcelona.[49] In Casas et al., 2020, ionizable perfluoroalkyl substances (PFAS) measured in maritime Antarctica exhibited EFs of 1.2 to 5 in the SML.[75] In one study by Karnatz et al., 2025, naturally occurring organic matter, including dissolved amino acids were enriched in the SML by a factor of 2.88, while the EF for glucose was 8.79, with enhancements in the EF during or following a phytoplankton bloom.[76] While our experiments did not grow a phytoplankton bloom, it is useful for comparing EFs with other organic molecules with different structure and moieties.

In nascent SSA generated by the MART, DBP was significantly more enriched than DMP. For DBP alone, the two trials showed EFs of 28800(±1300) on 7/25/25 and 16000(±7000) on 11/20/25, whereas DMP EF values were 6(±12) on the 7/22/25 trial and 450(±50) on the 11/18/25 trial. When mixed with all PAEs, DBP EF values were 57400(±2500) on 8/23/25 and

35000(±8000) on 12/13/25. In contrast, DMP EF values when mixed with all PAEs were 2.5(±1.0) on 8/23/25 and 542(±24) on 12/23/25.

While there are currently no other studies that have reported PAE EFs in SSA, others have reported significant enrichment of other organic contaminants. In Trilla-Prieto et al., 2024, they estimated EFs of organophosphate esters in SSA (based on previously measured concentrations in aerosols) ranged from 36,900 to 3,330,000.[48] In Casas et al., 2020, PFAS sampled in maritime Antarctica SSA exhibited EFs from 522 to 4,690, in the same order of magnitude as DMP and DBP in this study.[49]

Table 6. Concentrations and calculated EF values for DMP and DBP in different matrices.

Experiment	Concentration PAE Bulk (g/g)	Concentration Na+ Bulk (g/g)	Concentration PAE SSML (g/g)	Concentration Na+ SSML (g/g)	Concentration PAE Aerosol (g/m3)	Concentration Na+ Aerosol (g/m3)	EF SSA	EF SSM
DMP (25/07/22)	1.92E-07 ± 8.14E-09	0.010 ± 0.0002	2.15E-07 ± 9.14E-09	0.0110 ± 0.0006	3.68E-09 ± 6.86E-09	4.42E-06 ± 8.44E-07	6 ± 12	1.25 ± 0
DMP ALL PAE (25/08/23)	2.24E-07 ± 9.54E-09	0.0121 ± 0.0002	2.58E-07 ± 1.10E-08	0.0095 ± 0.0002	1.77E-08 ± 6.98E-09	3.88E-04 ± 5.49E-06	2.5 ± 1.0	1.47 ± 0
DBP (25/07/25)	8.638E-08 ± 2.309E-09	0.0131 ± 0.0003	5.169E-08 ± 1.513E-09	0.0119 ± 0.0004	6.430E-06 ± 1.720E-07	1.98E-04 ± 3.39E-05	28800 ± 1300	34.3 ± 1
DBP ALL PAE (25/08/23)	8.463E-08 ± 2.263E-09	0.0121 ± 0.0002	2.086E-07 ± 5.610E-09	0.0095 ± 0.0002	1.557E-04 ± 4.163E-06	3.88E-04 ± 5.49E-06	57400 ± 2500	21.1 ± (
DMP (25/11/18)	2.73E-06 ± 6.06E-08	0.0115 ± 0.0002	2.46E-06 ± 5.49E-08	0.0122 ± 0.0002	4.71E-07 ± 4.97E-08	4.42E-06 ± 8.15E-07	450 ± 50	5.45 ± 0
DMP ALL PAE (25/12/23)	1.77E-06 ± 3.95E-08	0.0145 ± 0.0003	2.10E-06 ± 4.72E-08	0.0117 ± 0.0002	1.26E-05 ± 6.61E-08	3.23E-05 ± 7.56E-07	542 ± 24	1.47 ± 0
DBP (25/11/20)	2.129E-08 ± 1.931E-09	0.0111 ± 0.0002	4.475E-07 ± 5.212E-08	0.0117 ± 0.0002	4.436E-07 ± 1.915E-07	1.46E-05 ± 9.71E-07	16000 ± 7000	20 ± 3
DBP ALL PAE (25/12/13)	1.674E-08 ± 1.525E-09	0.0145 ± 0.0003	2.108E-07 ± 3.598E-08	0.0117 ± 0.0002	7.630E-06 ± 2.647E-07	3.23E-05 ± 7.56E-07	35000 ± 8000	16 ± 3

3.3.1 Differences in the Enrichment of DBP compared to DMP in the sea surface layer and SSA

The greater enrichment of DBP compared to DMP in both the aerosol phase and SML may be attributed to several compounding factors, including differences in molecular size, hydrophobicity, volatility, and surface activity. Due to its longer alkyl chain, DBP has a significantly higher octanol/water partitioning coefficient (Log K_{ow}~4.5), as shown in Table 7, and specific gravity near 1 compared to DMP (Log K_{ow}~1.6), with a higher specific gravity, making it more available to be suspended in the water column and relatively less interaction with lipids in the SML. Based on the definition of K_{ow}, the concentration of DBP relative to DMP in octanol is approximately 800 times larger (i.e., $10^{4.5}/10^{1.6}$) compared to that in pure water. In comparison, the ratio of DBP to DMP in the SML samples in our experiments was approximately 3-34x greater compared to the underlying seawater. This highlights a key difference in the hydrophobicity of the samples in our experiments. Namely, palmitic acid exists in its more soluble de-protonated form in artificial seawater, whereas octanol lacks an acidic proton and is insoluble in water. Therefore, DBP would likely be less enriched in the more soluble palmitate SML than a pure octanol layer.

Table 7. Physiochemical properties of DMP, DBP, and DEHP.

PAE	**Molecular Weight g/mol**	**Specific Gravity (20°)**	**Log K_{ow}**	**VP (mmHg, 25°)**
DMP	194.2	1.192	1.46-1.90	2.0×10^{-3}
DBP	278.4	1.042	3.74-5.15	2.7×10^{-5}
DEHP	390.6	0.986	5.11-8.35	1.0×10^{-7}

Furthermore, DMP is more volatile than DBP, which means it can escape to the atmosphere directly via gas exchange rather than being carried upward in bubble films. The vapor pressure of DBP is 1.0×10^{-5} mmHg at 25°C, two orders of magnitude less than the vapor

pressure of DMP (4.19×10^{-3} mmHg at 20°C).[77] Due to its greater hydrophobicity, DBP can adhere more strongly to rising bubbles and therefore become scavenged more efficiently than DMP. This could explain the significantly higher ratios of DBP to DMP in the collected nascent SSA, which range from 29x to 29,000x greater than in the underlying seawater. The study by Cooper et al., 2025 showed that the aerosol-to-water ratios of several contaminants of emerging concern in field samples in coastal San Diego, California increased with their hydrophobicity.[46]

3.3.2 Potential Reasons for Variability in the EF between Trials

There were significant differences in the EF values between trials for the PAE systems studied. Most notable are the differences in the EFs of DMP in nascent SSA, which varied by two orders of magnitude between trials for both DMP alone and DMP mixed with all PAEs. We will focus on DMP, as the EFs of DBP between trials, although different, were all within the same order of magnitude. When examining the aerosol size distributions between trials (Fig. 15), there are clear differences in both the total aerosol concentration and the size of nascent SSA that was generated. For example, on 11/18/25 (DMP EF = 450±50), there is a single number weighted size mode of ~50 nm (orange plot in Fig. 15A), whereas on 7/22/25 (DMP EF=6±12) there were three apparent modes of ~70 nm, ~120 nm, and >~300 nm (red plot in Fig. 15A). While the nascent SSA size distributions for the DBP experiments varied too, each exhibited one larger and one smaller size mode. On 11/20/25 (DBP EF=16000±7000), the broader smaller mode peaked at ~35 nm and the larger mode peaked at ~400 nm (purple in Fig. 15B). In comparison, on 7/25/25 (DBP EF=28800±1300), the size distribution was like that for DMP on 7/22/25, with a smaller mode ~120 nm and a larger mode >~300 nm (teal in Fig. 15B). This importantly demonstrates a possible size dependence in the EF of the PAEs studied here. Several

studies have observed a similar size dependence in the level of enrichment of other chemical species in aerosols. For example, the enrichment of divalent cations (Mg^{2+} and Ca^{2+}) in nascent SSA is greater with smaller aerosol diameter.[35] There are other examples of the enrichment of transparent exopolymers (TEP) in smaller SSA particles collected from field samples in the North Atlantic and greater mass fractions of organic carbon in smaller SSA.[53,78] In Fang et al., 2025, various types of perfluoroalkyl substances exhibited size dependent EFs in artificial lab SSA and field-collected samples, with an order of magnitude greater EF in 100-200 nm SSA compared to 500 nm SSA..[51] Here, like in these other studies, the smaller SSA particles generated in the MART contain a greater fraction of organic material (i.e., PAEs), resulting from the bursting surface film, which is enriched in surface active material. The MART experiments producing a larger fraction of smaller SSA (or smaller fraction of larger SSA) would contain relatively larger fractions of PAEs. [5051]

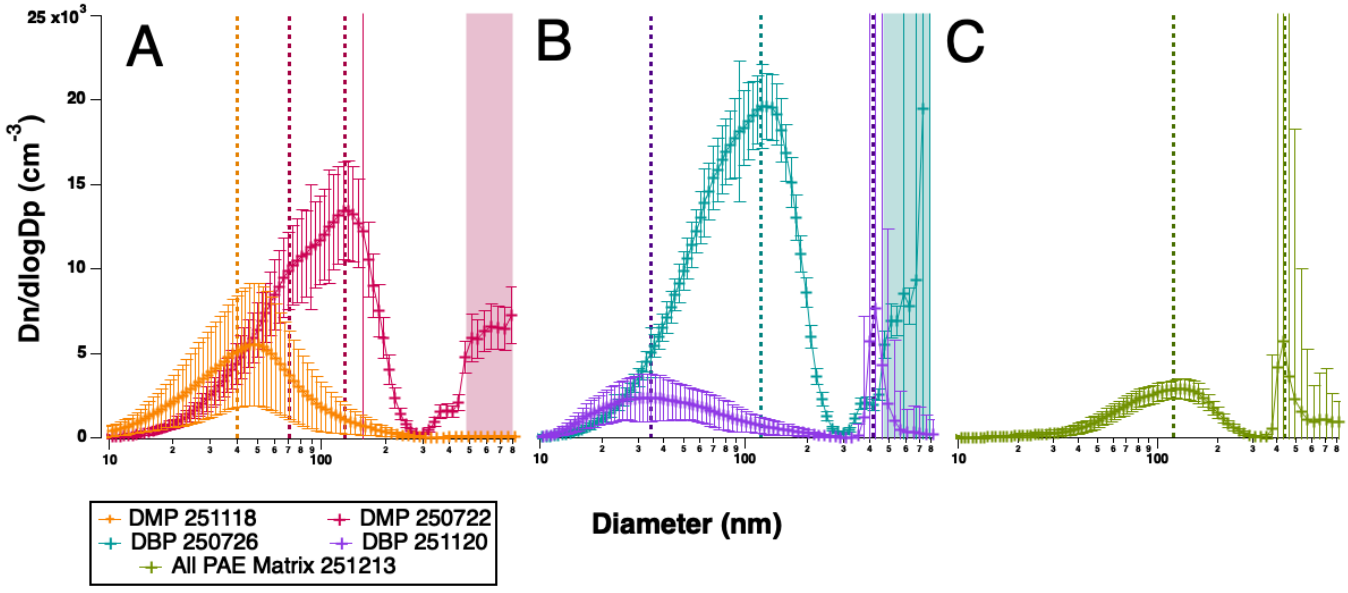

Figure 15. Particle size distributions of A. DMP matrix experiments, B. DBP matrix experiments, and C. all PAE matrix experiment. Only one experiment is plotted due to the instrument being under repair. Concentration of particles (Dn/dlogDp) is plotted versus particle diameter. Error bars illustrate the concentrations standard deviation. The vertical bars (dashed) indicate the position of the different size distribution peaks (modes).x

3.4 DEHP Analysis

The results from the DEHP data were inconclusive, and no EF values were able to be calculated. In the DEHP experiments, when only DEHP was added to the matrix, the samples contained apparently less DEHP than the blank samples, as shown in Fig 16. The mass spectral analysis resulted in high concentrations of DBP being detected when only DEHP was added to the matrix. This was true for the matrix of DEHP alone, and with DMP and DBP.

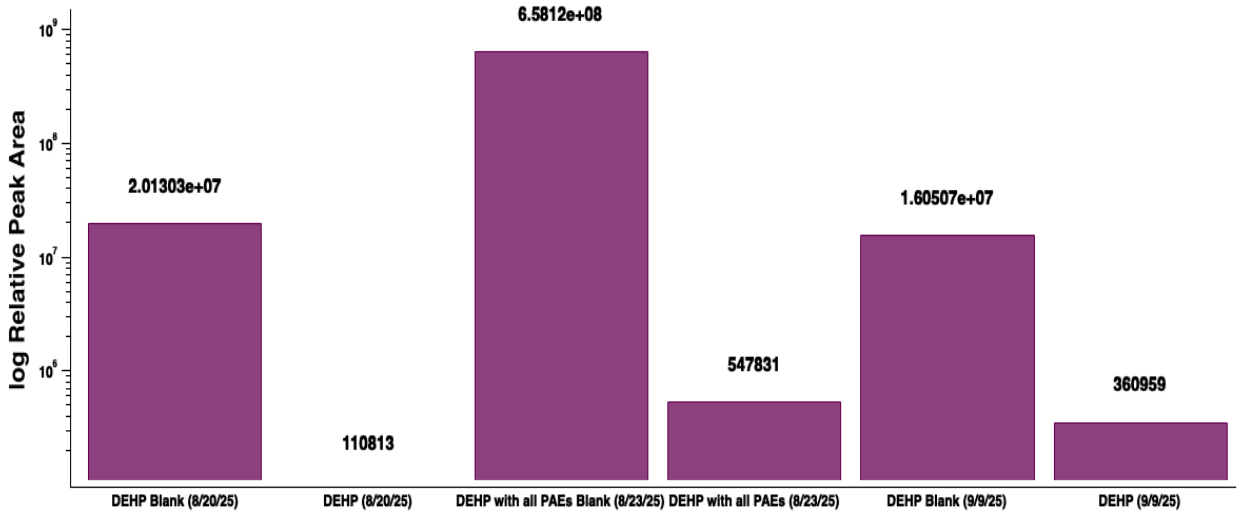

Figure 16. Relative peak area signal from DEHP filter extractions. Signal intensity for filter blanks were consistently higher in DEHP signal than the sample filters.

The reasons for this are not clear. It may be related to fragmentation in the MS. In general, phthalates form similar fragmentation patterns through either the McLafferty+1 rearrangement or the loss of the alkoxy.[79] In complex matrices, it can be difficult to distinguish different phthalates from each other using EI MS.[80] However, the GC/MS data was cross-referenced, confirming that the signal was from DBP even with having the same quantification fragment of 149 m/z. Fig. 17 displays the concentrations in g/g from filter extractions from a DEHP matrix, and a matrix with all PAEs. The filter blanks for DEHP have higher signal than the actual filter samples, making

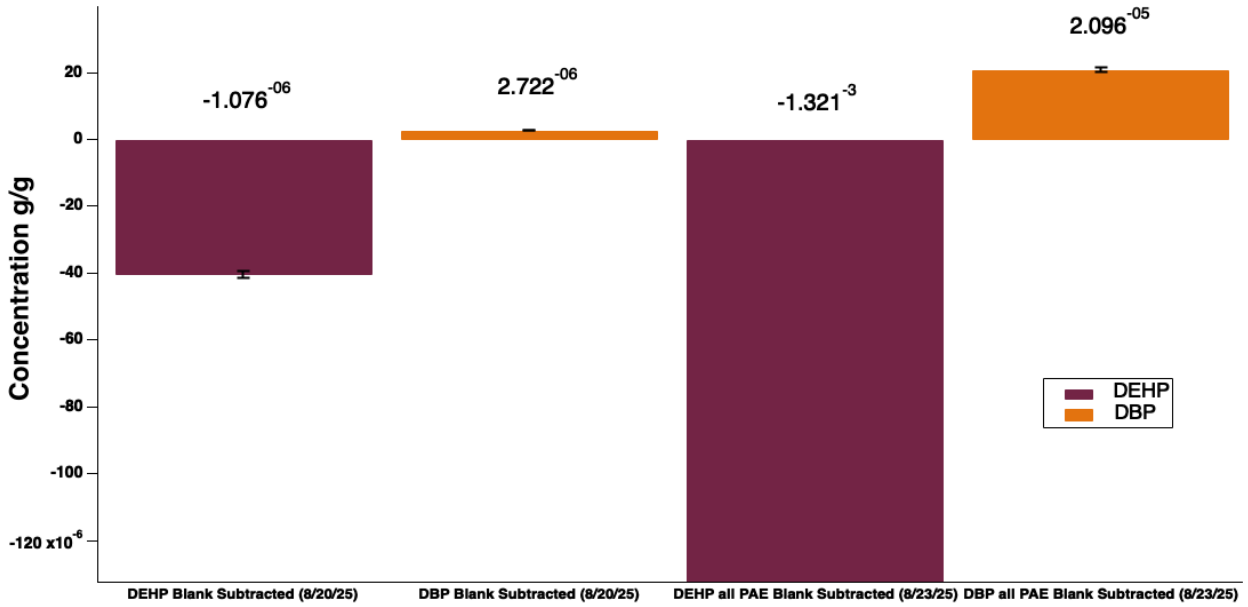

Figure 17. Concentrations of DEHP and DBP from a DEHP matrix and a matrix with all PAEs. Filter blanks have been subtracted from filter samples.

the concentration negative in the sample. The signal for DBP is what is expected, the filter blank has contamination, but the signal for the actual sample is much higher. The results from the DBP confirms that no human error, such as mislabeling samples was the reason for this anomaly. Data from the DEHP experiments consistently showed higher signal in the blanks and SW matrices without DEHP added; the signal from DBP from these samples showed what was expected, low signal in blanks, and high signal in the sample. DEHP was unable to be calculated in the final total PAE experiment due to GC/MS signal shifts. This indicates systematic error in DEHP data collection and experiments. Signal intensity for SW and sea surface layer samples also varied. Most experiments show higher signals for DEHP in the blank, and high signals for DBP when DEHP was added. Overall, the data for DEHP did not have a detectable trend and was inconsistent in all matrices.

Degradation pathways for DEHP have been studied but are unlikely representative of the experiments. In Staples et al. 1997, DEHP degraded by photo-oxidation and hydrolysis with half-lives of .2-2 days and 2000 years, respectively.[17] Many studies show biodegradation of DEHP within the presence of biotic factors, and can form the corresponding phthalate monomers and DBP; however, as no biological components were in this experiment, this degradation pathway can be ruled out.[19,81,82] This is a subject of future work.

3.5 Implications

Our findings show that phthalate esters are substantially enriched in both the sea surface microlayer and sea spray aerosols relative to bulk seawater, demonstrating that the ocean-atmosphere interface is an active and efficient pathway for their atmospheric emission. DBP exhibits EFs far greater than those of DMP and comparable to those reported for highly surface-active PFAS, indicating that DBP is especially prone to bubble-mediated transfer into the air. These results highlight that phthalates are not merely dissolved contaminants but can be selectively concentrated and aerosolized, with important implications for the environmental fate and potential human exposure.

Once airborne, PAEs can undergo long-range transport, oxidation, and deposition back to the ocean or land, with atmospheric lifetimes ranging from hours to months depending on molecular structure.[17] Although the effects of PAEs in the atmosphere remain poorly constrained, our work provides quantitative evidence that they are efficiently injected into the air and therefore capable of participating in atmospheric processes. Recent observations of microplastics acting as cloud condensation nuclei and ice-nucleating particles, along with their measurable radiative forcing, underscore the need to understand whether aerosolized phthalates similarly influence cloud formation or the radiative balance. [83,84,85] Given the global production of PAEs reaching 6 – 8 million tons and their integration into nearly all environmental compartments, determining how phthalates in SSA affect CCN activity, INP behavior, and atmospheric scattering and absorption represents an important next step. [67,86] Future studies should expand measurements to additional phthalate species, assess their chemical evolution once airborne, and evaluate their impacts on atmospheric processes and human health.

Chapter 3, in part, coauthored with Slade, Jonathan H., is currently being prepared for submission under the title, “Phthalate Transfer and Enrichment in Artificial Sea Spray Aerosols.” The thesis author is the primary author of this chapter.

Chapter 4: Conclusions and Future Work

4.1 Conclusions

The identification from past studies of PAEs in many parts of the ocean and atmosphere, indicate a transfer occurring via evaporation, or SSA. This study investigated the transport of PAEs via SSA from artificial seawater. The experiments, conducted in a MART, utilized varying matrices to identify different transfer aspects of PAEs. EF values were calculated for SSA and the sea surface layer, for both individual PAs matrices, and when all the PAEs were present. The EF values found, for DMP and DBP, two of the three PAEs used in the study, provide insight into the fate of PAEs in the ocean.

The EF values calculated for DMP exhibited a slight preference for transfer via SSA and no great difference when mixed with other PAEs. In two independent MART experiments, DMP EFs exhibited a two-order of magnitude difference. The particle size distributions also differed between experiments and the results suggested particle size plays a critical role in enrichment. DBP was preferentially transferred in SSA compared to DMP, with EF values in the tens of thousands. Again, the data sets differed in values, and the SEMS data provided different size distributions. Unlike DMP, DBP showed a significant difference in EF values between trials with and without other PAEs. It was found that DBP is more likely to transfer when present with other similar surface-active PAE species.

Sea surface layer EF values for DMP displayed a slight enrichment across all experiments. With a low specific gravity near 1, DMP is expected to be suspended in the water column rather than on the surface, consistent with the lower measured EF. DBP was found to have a higher SML EF value than DMP. In the matrix with other PAEs, the EF values were calculated to be lower than on its own, but on the same order of magnitude. These trends were

consistent between trials. It was expected that DBP would be more enriched than DMP in the sea surface layer because of a high Log K_{ow}, making it more likely to interact with hydrophobic species.

The results for the DEHP studies remain inconclusive. Signal intensity varied and had no distinct relationship between blanks, filter sample collection, and bulk water samples. While DBP signal was present in DEHP experiments, it is unknown why this is occurring. This subject requires further investigation to fully comprehend the behavior of DEHP.

4.2 Future Work

This study provided insight into the behavior of PAEs in in the ocean. The calculated EF values are foundational to understanding the long-term effects of PAEs in our environment. Many additional studies should expand upon the data collected, and aid in completing a broader representation of the fate of PAEs. Below are suggested future directions including (1) improving methodologies for detection of longer-chained PAEs including DEHP, (2) size-dependent studies, (3) representative sea surface conditions, and (4) introducing atmospheric chemistry.

The EF value of DEHP was unable to be calculated for reasons including high backgrounds and potential degradation of DEHP in the sample forming DBP. The GC/MS temperature ramp used for PAE detection did not reach a temperature at which other papers measured DEHP.[60,61,87] Increasing the final temperature from 250°C to 280°C may improve DEHP detectability. To improve detection of DEHP, a different temperature ramp with an increased maximum temperature is suggested. Mi et al. 2023 utilizes a temperature ramp increased to 280°C. Paluselli et al. 2018 also uses a program that reaches 280°C. Both studies detected DEHP without issue.[13,60] Other studies should be conducted of the degradation of DEHP under various conditions. Other MART studies use nitrogen as a carrier gas, where this study used a ZAG.[54,88] Nitrogen is relatively inert gas under normal conditions and does not readily react with compounds. This could lead to interesting results and perhaps shed light on some of the properties of DEHP in SSA.

The SEMS data collected had varied results between experiments. The particle size distributions and correlated EF values indicated that there might be a size correlation to EF values of PAEs. SSA composition is dependent on size and can vastly alter the properties.[44] This

work is currently being investigated by our group. Utilizing an electrical low-pressure impactor (ELPI), different aerosol particle sizes are collected on the collection plates, allowing particle size specific EF values to be calculated. This will provide information on the behavior of PAEs in size specific particles.

Palmitic acid was used as a SSML proxy in the MART experiments to replicate real environmental conditions. To expand upon the environmental relevance of this study, other components should be added to the matrix, such as phytoplankton blooms. Biological activity could lead to different SSA enrichment, as well as unidentified chemistry in this study. Biodegradation and bioaccumulation is a common fate of PAEs in many systems and could have a significant impact on the EF values of PAEs.[89,90]

This study focused on how PAEs transfer into the atmosphere via SSA. To further investigate the effects that PAEs have on our environment, air chemistry experiments should be explored. Instruments such as the Potential Aerosol Mass Oxidation Flow Reactor (PAM-OFR), would allow targeted degradation experiments to be conducted. Using a PAM-OFR, photochemical reactions, and heterogeneous oxidative reactions can be studied.[91] Photodegradation of PAEs has been identified to occur in water and in the air, but specifics on SSA chemistry remain unknown.[17,92,93] Feng et al. 2022 describes chlorinated photoproducts of DMP from studies conducted in DCM.[92] SSA being an abundant source of Cl^-, could promote high concentrations of chlorinated PAE products.[91] The results of these experiments will aid in understanding the behavior of PAEs in the aerosols, and the impact they have on our atmosphere.

Chapter 4, in part, coauthored with Slade, Jonathan H., is currently being prepared for submission under the title, “Phthalate Transfer and Enrichment in Artificial Sea Spray Aerosols.” The thesis author is the primary author of this chapter.

REFERENCES

(1) Graham, P. R. Phthalate Ester Plasticizers--Why and How They Are Used. *Environ. Health Perspect.* **1973**, *3*, 3–12. https://doi.org/10.1289/ehp.73033.

(2) Warner, G. R.; Flaws, J. A. Bisphenol A and Phthalates: How Environmental Chemicals Are Reshaping Toxicology. *Toxicol. Sci.* **2018**, *166* (2), 246–249. https://doi.org/10.1093/toxsci/kfy232.

(3) Giuliani, A.; Zuccarini, M.; Cichelli, A.; Khan, H.; Reale, M. Critical Review on the Presence of Phthalates in Food and Evidence of Their Biological Impact. *Int. J. Environ. Res. Public. Health* **2020**, *17* (16), 5655. https://doi.org/10.3390/ijerph17165655.

(4) Oca, M. L.; Rubio, L.; Sarabia, L. A.; Ortiz, M. C. Dealing with the Ubiquity of Phthalates in the Laboratory When Determining Plasticizers by Gas Chromatography/Mass Spectrometry and PARAFAC. *J. Chromatogr. A* **2016**, *1464*, 124–140. https://doi.org/10.1016/j.chroma.2016.07.074.

(5) Luo, Q.; Liu, Z.; Yin, H.; Dang, Z.; Wu, P.; Zhu, N.; Lin, Z.; Liu, Y. Migration and Potential Risk of Trace Phthalates in Bottled Water: A Global Situation. *Water Res.* **2018**, *147*, 362–372. https://doi.org/10.1016/j.watres.2018.10.002.

(6) Mansuri, A.; Trivedi, C.; Chokshi, S.; Jantrania, K.; Kumar, A. Phthalate Exposure: Prevalence, Health Effects, Regulatory Frameworks, and Remediation. *Chem. Res. Toxicol.* **2025**, *38* (8), 1291–1308. https://doi.org/10.1021/acs.chemrestox.4c00338.

(7) Marx, J. L. Phthalic Acid Esters: Biological Impact Uncertain. *Science* **1972**, *178* (4056), 46–47.

(8) Apau, J.; Sefah, W.; Adua, E. Human Contact with Phthalates during Early Life Stages Leads to Weight Gain and Obesity. *Cogent Chem.* **2020**, *6* (1), 1815273. https://doi.org/10.1080/23312009.2020.1815273.

(9) Net, S.; Sempéré, R.; Delmont, A.; Paluselli, A.; Ouddane, B. Occurrence, Fate, Behavior and Ecotoxicological State of Phthalates in Different Environmental Matrices. *Environ. Sci. Technol.* **2015**, *49* (7), 4019–4035. https://doi.org/10.1021/es505233b.

(10) Paluselli, A.; Fauvelle, V.; Galgani, F.; Sempéré, R. Phthalate Release from Plastic Fragments and Degradation in Seawater. *Environ. Sci. Technol.* **2019**, *53* (1), 166–175. https://doi.org/10.1021/acs.est.8b05083.

(11) Hidalgo-Serrano, M.; Borrull, F.; Marcé, R. M.; Pocurull, E. Phthalate Esters in Marine Ecosystems: Analytical Methods, Occurrence and Distribution. *TrAC Trends Anal. Chem.* **2022**, *151*, 116598. https://doi.org/10.1016/j.trac.2022.116598.

(12) Billings, A.; Jones, K. C.; Pereira, M. G.; Spurgeon, D. J. Emerging and Legacy Plasticisers in Coastal and Estuarine Environments: A Review. *Sci. Total Environ.* **2024**, *908*, 168462. https://doi.org/10.1016/j.scitotenv.2023.168462.

(13) Mi, L.; Xie, Z.; Xu, W.; Waniek, J. J.; Pohlmann, T.; Mi, W. Air–Sea Exchange and Atmospheric Deposition of Phthalate Esters in the South China Sea. *Environ. Sci. Technol.* **2023**, *57* (30), 11195–11205. https://doi.org/10.1021/acs.est.2c09426.

(14) Xie, Z.; Ebinghaus, R.; Temme, C.; Caba, A.; Ruck, W. Atmospheric Concentrations and Air–Sea Exchanges of Phthalates in the North Sea (German Bight). *Atmos. Environ.* **2005**, *39* (18), 3209–3219. https://doi.org/10.1016/j.atmosenv.2005.02.021.

(15) Xie, Z.; Ebinghaus, R.; Temme, C.; Lohmann, R.; Caba, A.; Ruck, W. Occurrence and Air−Sea Exchange of Phthalates in the Arctic. *Environ. Sci. Technol.* **2007**, *41* (13), 4555–4560. https://doi.org/10.1021/es0630240.

(16) Wang, L.-Y.; Gu, Y.-Y.; Zhang, Z.-M.; Sun, A.-L.; Shi, X.-Z.; Chen, J.; Lu, Y. Contaminant Occurrence, Mobility and Ecological Risk Assessment of Phthalate Esters in the Sediment-Water System of the Hangzhou Bay. *Sci. Total Environ.* **2021**, *770*, 144705. https://doi.org/10.1016/j.scitotenv.2020.144705.

(17) Staples, C. A.; Peterson, D. R.; Parkerton, T. F.; Adams, W. J. The Environmental Fate of Phthalate Esters: A Literature Review. *Chemosphere* **1997**, *35* (4), 667–749. https://doi.org/10.1016/S0045-6535(97)00195-1.

(18) Wolfe, N. L.; Steen, W. C.; Burns, L. A. Phthalate Ester Hydrolysis: Linear Free Energy Relationships. *Chemosphere* **1980**, *9* (7–8), 403–408. https://doi.org/10.1016/0045-6535(80)90023-5.

(19) Chang, B. V.; Liao, C. S.; Yuan, S. Y. Anaerobic Degradation of Diethyl Phthalate, Di-n-Butyl Phthalate, and Di-(2-Ethylhexyl) Phthalate from River Sediment in Taiwan. *Chemosphere* **2005**, *58* (11), 1601–1607. https://doi.org/10.1016/j.chemosphere.2004.11.031.

(20) Peng, X.; Feng, L.; Li, X. Pathway of Diethyl Phthalate Photolysis in Sea-Water Determined by Gas Chromatography–Mass Spectrometry and Compound-Specific Isotope Analysis. *Chemosphere* **2013**, *90* (2), 220–226. https://doi.org/10.1016/j.chemosphere.2012.06.045.

(21) Behnke, W.; Nolting, F.; Zetzsch, C. THE ATMOSPHERIC FATE OF DI(2-ET~)PHTHALATE, ADSORBED ON VARIOUS ~-'fAL OXIDE MODEL AEROSOLS AND ON COAL FLY ASH.

(22) Scholz, N. Ecotoxicity and Biodegradation of Phthalate Monoesters. *Chemosphere* **2003**, *53* (8), 921–926. https://doi.org/10.1016/S0045-6535(03)00668-4.

(23) Wang, Y.; Qian, H. Phthalates and Their Impacts on Human Health. *Healthcare* **2021**, *9* (5), 603. https://doi.org/10.3390/healthcare9050603.

(24) Khoshmanesh, M.; Farjadfard, S.; Ahmadi, M.; Ramavandi, B.; Fatahi, M.; Sanati, A. M. Review of Toxicity and Global Distribution of Phthalate Acid Esters in Fish. *Sci. Total Environ.* **2024**, *953*, 175966. https://doi.org/10.1016/j.scitotenv.2024.175966.

(25) Latini, G. Monitoring Phthalate Exposure in Humans. *Clin. Chim. Acta* **2005**, *361* (1–2), 20–29. https://doi.org/10.1016/j.cccn.2005.05.003.

(26) Wang, Y.; Zhu, H.; Kannan, K. A Review of Biomonitoring of Phthalate Exposures. *Toxics* **2019**, *7* (2), 21. https://doi.org/10.3390/toxics7020021.

(27) Kolatorova, L.; Vitku, J.; Vavrous, A.; Hampl, R.; Adamcova, K.; Simkova, M.; Parizek, A.; Starka, L.; Duskova, M. Phthalate Metabolites in Maternal and Cord Plasma and Their Relations to Other Selected Endocrine Disruptors and Steroids. *Physiol. Res.* **2018**, S473–S487. https://doi.org/10.33549/physiolres.933962.

(28) Park, C.-B.; Kim, G.-E.; Kim, Y. J.; On, J.; Park, C.-G.; Kwon, Y.-S.; Pyo, H.; Yeom, D.-H.; Cho, S.-H. Reproductive Dysfunction Linked to Alteration of Endocrine Activities in Zebrafish Exposed to Mono-(2-Ethylhexyl) Phthalate (MEHP). *Environ. Pollut.* **2020**, *265*, 114362. https://doi.org/10.1016/j.envpol.2020.114362.

(29) Wen, Z.-J.; Wang, Z.-Y.; Zhang, Y.-F. Adverse Cardiovascular Effects and Potential Molecular Mechanisms of DEHP and Its Metabolites—A Review. *Sci. Total Environ.* **2022**, *847*, 157443. https://doi.org/10.1016/j.scitotenv.2022.157443.

(30) Keith, L.; Telliard, W. ES&T Special Report: Priority Pollutants: I-a Perspective View. *Environ. Sci. Technol.* **1979**, *13* (4), 416–423. https://doi.org/10.1021/es60152a601.

(31) US EPA, O. *EPA Announces Intent to Regulate Dozens of Uses of Five Phthalate Chemicals to Protect Workers and Environment*. https://www.epa.gov/newsreleases/epa-announces-intent-regulate-dozens-uses-five-phthalate-chemicals-protect-workers-and (accessed 2026-03-18).

(32) Net, S.; Delmont, A.; Sempéré, R.; Paluselli, A.; Ouddane, B. Reliable Quantification of Phthalates in Environmental Matrices (Air, Water, Sludge, Sediment and Soil): A Review. *Sci. Total Environ.* **2015**, *515–516*, 162–180. https://doi.org/10.1016/j.scitotenv.2015.02.013.

(33) Paluselli, A.; Kim, S.-K. Horizontal and Vertical Distribution of Phthalates Acid Ester (PAEs) in Seawater and Sediment of East China Sea and Korean South Sea: Traces of Plastic Debris? *Mar. Pollut. Bull.* **2020**, *151*, 110831. https://doi.org/10.1016/j.marpolbul.2019.110831.

(34) Benson, N. U.; Fred-Ahmadu, O. H. Occurrence and Distribution of Microplastics-Sorbed Phthalic Acid Esters (PAEs) in Coastal Psammitic Sediments of Tropical Atlantic Ocean, Gulf of Guinea. *Sci. Total Environ.* **2020**, *730*, 139013. https://doi.org/10.1016/j.scitotenv.2020.139013.

(35) Bertram, T. H.; Cochran, R. E.; Grassian, V. H.; Stone, E. A. Sea Spray Aerosol Chemical Composition: Elemental and Molecular Mimics for Laboratory Studies of Heterogeneous and Multiphase Reactions. *Chem. Soc. Rev.* **2018**, *47* (7), 2374–2400. https://doi.org/10.1039/C7CS00008A.

(36) de Leeuw, G.; Andreas, E. L.; Anguelova, M. D.; Fairall, C. W.; Lewis, E. R.; O'Dowd, C.; Schulz, M.; Schwartz, S. E. Production Flux of Sea Spray Aerosol. *Rev. Geophys.* **2011**, *49* (2). https://doi.org/10.1029/2010RG000349.

(37) Cochran, R. E.; Ryder, O. S.; Grassian, V. H.; Prather, K. A. Sea Spray Aerosol: The Chemical Link between the Oceans, Atmosphere, and Climate. *Acc. Chem. Res.* **2017**, *50* (3), 599–604. https://doi.org/10.1021/acs.accounts.6b00603.

(38) Sauer, J. S.; Mayer, K. J.; Lee, C.; Alves, M. R.; Amiri, S.; Bahaveolos, C. J.; Franklin, E. B.; Crocker, D. R.; Dang, D.; Dinasquet, J.; Garofalo, L. A.; Kaluarachchi, C. P.; Kilgour, D. B.; Mael, L. E.; Mitts, B. A.; Moon, D. R.; Moore, A. N.; Morris, C. K.; Mullenmeister, C. A.; Ni, C.-M.; Pendergraft, M. A.; Petras, D.; Simpson, R. M. C.; Smith, S.; Tumminello, P. R.; Walker, J. L.; DeMott, P. J.; Farmer, D. K.; Goldstein, A. H.; Grassian, V. H.; Jaffe, J. S.; Malfatti, F.; Martz, T. R.; Slade, J. H.; Tivanski, A. V.; Bertram, T. H.; Cappa, C. D.; Prather, K. A. The Sea Spray Chemistry and Particle Evolution Study (SeaSCAPE): Overview and Experimental Methods. *Environ. Sci. Process. Impacts* **2022**, *24* (2), 290–315. https://doi.org/10.1039/D1EM00260K.

(39) Wang, X.; Deane, G. B.; Moore, K. A.; Ryder, O. S.; Stokes, M. D.; Beall, C. M.; Collins, D. B.; Santander, M. V.; Burrows, S. M.; Sultana, C. M.; Prather, K. A. The Role of Jet and Film Drops in Controlling the Mixing State of Submicron Sea Spray Aerosol Particles. *Proc. Natl. Acad. Sci.* **2017**, *114* (27), 6978–6983. https://doi.org/10.1073/pnas.1702420114.

(40) Lee, H. D.; Wigley, S.; Lee, C.; Or, V. W.; Hasenecz, E. S.; Stone, E. A.; Grassian, V. H.; Prather, K. A.; Tivanski, A. V. Physicochemical Mixing State of Sea Spray Aerosols: Morphologies Exhibit Size Dependence. *ACS Earth Space Chem.* **2020**, *4* (9), 1604–1611. https://doi.org/10.1021/acsearthspacechem.0c00153.

(41) Chingin, K.; Yan, R.; Zhong, D.; Chen, H. Enrichment of Surface-Active Compounds in Bursting Bubble Aerosols. *ACS Omega* **2018**, *3* (8), 8709–8717. https://doi.org/10.1021/acsomega.8b01157.

(42) Cunliffe, M.; Engel, A.; Frka, S.; Gašparović, B.; Guitart, C.; Murrell, J. C.; Salter, M.; Stolle, C.; Upstill-Goddard, R.; Wurl, O. Sea Surface Microlayers: A Unified

Physicochemical and Biological Perspective of the Air–Ocean Interface. *Prog. Oceanogr.* **2013**, *109*, 104–116. https://doi.org/10.1016/j.pocean.2012.08.004.

(43) Schill, S. R.; Burrows, S. M.; Hasenecz, E. S.; Stone, E. A.; Bertram, T. H. The Impact of Divalent Cations on the Enrichment of Soluble Saccharides in Primary Sea Spray Aerosol. *Atmosphere* **2018**, *9* (12), 476. https://doi.org/10.3390/atmos9120476.

(44) Ault, A. P.; Moffet, R. C.; Baltrusaitis, J.; Collins, D. B.; Ruppel, M. J.; Cuadra-Rodriguez, L. A.; Zhao, D.; Guasco, T. L.; Ebben, C. J.; Geiger, F. M.; Bertram, T. H.; Prather, K. A.; Grassian, V. H. Size-Dependent Changes in Sea Spray Aerosol Composition and Properties with Different Seawater Conditions. *Environ. Sci. Technol.* **2013**, *47* (11), 5603–5612. https://doi.org/10.1021/es400416g.

(45) Cochran, R. E.; Jayarathne, T.; Stone, E. A.; Grassian, V. H. Selectivity Across the Interface: A Test of Surface Activity in the Composition of Organic-Enriched Aerosols from Bubble Bursting. *J. Phys. Chem. Lett.* **2016**, *7* (9), 1692–1696. https://doi.org/10.1021/acs.jpclett.6b00489.

(46) Cooper, A.; Cancelada, L.; Riley Torres, R.; Belcher, K.; Small, M.; Belda-Ferre, P.; Morris, C.; Mitts, B.; Dinasquet, J.; Knight, R.; Slade, J. H.; Prather, K. A. *Identifying wastewater chemicals in coastal aerosols*. https://doi.org/10.1126/sciadv.ads9476.

(47) Baylor, E. R.; Baylor, M. B.; Blanchard, D. C.; Syzdek, L. D.; Appel, C. Virus Transfer from Surf to Wind. *Science* **1977**, *198* (4317), 575–580.

(48) Trilla-Prieto, N.; Iriarte, J.; Berrojalbiz, N.; Casas, G.; Sobrino, C.; Vila-Costa, M.; Jiménez, B.; Dachs, J. Enrichment of Organophosphate Esters in the Sea Surface Microlayer from the Atlantic and Southern Oceans. *Environ. Sci. Technol. Lett.* **2024**, *11* (9), 1008–1015. https://doi.org/10.1021/acs.estlett.4c00636.

(49) Casas, G.; Martínez-Varela, A.; Roscales, J. L.; Vila-Costa, M.; Dachs, J.; Jiménez, B. Enrichment of Perfluoroalkyl Substances in the Sea-Surface Microlayer and Sea-Spray Aerosols in the Southern Ocean. *Environ. Pollut.* **2020**, *267*, 115512. https://doi.org/10.1016/j.envpol.2020.115512.

(50) Reth, M.; Berger, U.; Broman, D.; Cousins, I. T.; Nilsson, E. D.; McLachlan, M. S. Water-to-Air Transfer of Perfluorinated Carboxylates and Sulfonates in a Sea Spray Simulator. *Environ. Chem.* **2011**, *8* (4), 381–388. https://doi.org/10.1071/EN11007.

(51) Fang, B.; Qiao, B.; Zhao, M.; Guo, J.; Wang, Y.; Yao, Y.; Chen, H.; Sun, H. The Accumulation of Per- and Polyfluoroalkyl Substances (PFAS) at the Air−water Interface: A Systematic Review. *J. Hazard. Mater.* **2025**, *494*, 138728. https://doi.org/10.1016/j.jhazmat.2025.138728.

(52) Liu, X.; Gao, Q.; Zhao, F.; Jiang, X.; Ma, X.; Yang, S.; Zhu, Y.; Wang, Z.; Huang, K.; Lu, X.; Wang, X. Sea Surface Temperature: A Key Regulator of Global Perfluoroalkyl Acids

Transport across the Sea–Air Interface. *Environ. Sci. Technol. Lett.* **2026**, *13* (1), 123–129. https://doi.org/10.1021/acs.estlett.5c01094.

(53) Tumminello, P. R.; Niles, R.; Valdez, V.; Madawala, C. K.; Gamage, D. K.; Kimble, K. A.; Leibensperger, R. J.; Huang, C.; Kaluarachchi, C.; Dinasquet, J.; Malfatti, F.; Lee, C.; Deane, G. B.; Stokes, M. D.; Stone, E.; Tivanski, A.; Prather, K. A.; Boor, B. E.; Slade, J. H. Size-Dependent Nascent Sea Spray Aerosol Bounce Fractions and Estimated Viscosity: The Role of Divalent Cation Enrichment, Surface Tension, and the Kelvin Effect. *Environ. Sci. Technol.* **2024**, *58* (44), 19666–19678. https://doi.org/10.1021/acs.est.4c04312.

(54) Stokes, M. D.; Deane, G. B.; Prather, K.; Bertram, T. H.; Ruppel, M. J.; Ryder, O. S.; Brady, J. M.; Zhao, D. A Marine Aerosol Reference Tank System as a Breaking Wave Analogue for the Production of Foam and Sea-Spray Aerosols. *Atmospheric Meas. Tech.* **2013**, *6* (4), 1085–1094. https://doi.org/10.5194/amt-6-1085-2013.

(55) Catarino, A. I.; León, M. C.; Li, Y.; Lambert, S.; Vercauteren, M.; Asselman, J.; Janssen, C. R.; Everaert, G.; De Rijcke, M. Micro- and Nanoplastics Transfer from Seawater to the Atmosphere through Aerosolization under Controlled Laboratory Conditions. *Mar. Pollut. Bull.* **2023**, *192*, 115015. https://doi.org/10.1016/j.marpolbul.2023.115015.

(56) Sellegri, K.; O'Dowd, C. D.; Yoon, Y. J.; Jennings, S. G.; de Leeuw, G. Surfactants and Submicron Sea Spray Generation. *J. Geophys. Res. Atmospheres* **2006**, *111* (D22). https://doi.org/10.1029/2005JD006658.

(57) Lee, C.; Sultana, C. M.; Collins, D. B.; Santander, M. V.; Axson, J. L.; Malfatti, F.; Cornwell, G. C.; Grandquist, J. R.; Deane, G. B.; Stokes, M. D.; Azam, F.; Grassian, V. H.; Prather, K. A. Advancing Model Systems for Fundamental Laboratory Studies of Sea Spray Aerosol Using the Microbial Loop. *J. Phys. Chem. A* **2015**, *119* (33), 8860–8870. https://doi.org/10.1021/acs.jpca.5b03488.

(58) Calvo, B.; Collado, I.; Cepeda, E. A. Solubilities of Palmitic Acid in Pure Solvents and Its Mixtures. *J. Chem. Eng. Data* **2009**, *54* (1), 64–68. https://doi.org/10.1021/je8005979.

(59) Cunliffe, M.; Wurl, O. *Guide to best practices to study the ocean's surface*. ResearchGate. https://www.researchgate.net/publication/266088134_Guide_to_best_practices_to_study_the_ocean%27s_surface#fullTextFileContent (accessed 2025-11-04).

(60) Paluselli, A.; Aminot, Y.; Galgani, F.; Net, S.; Sempere, R. Occurrence of Phthalate Acid Esters (PAEs) in the Northwestern Mediterranean Sea and the Rhone River. *Prog. Oceanogr.* **2018**, *163*, 221–231. https://doi.org/10.1016/j.pocean.2017.06.002.

(61) Paluselli, A.; Fauvelle, V.; Schmidt, N.; Galgani, F.; Net, S.; Sempéré, R. Distribution of Phthalates in Marseille Bay (NW Mediterranean Sea). *Sci. Total Environ.* **2018**, *621*, 578–587. https://doi.org/10.1016/j.scitotenv.2017.11.306.

(62) Li, D.; Stevens, R.; English, C. GC-MS Analysis of Phthalates: Comparison of GC Stationary Phase Performance.

(63) Duce, R. A.; Stumm, W.; Prospero, J. M. Working Symposium on Sea-Air Chemistry: Summary and Recommendations. *J. Geophys. Res. 1896-1977* **1972**, *77* (27), 5059–5061. https://doi.org/10.1029/JC077i027p05059.

(64) Yin, P.; Chen, H.; Liu, X.; Wang, Q.; Jiang, Y.; Pan, R. Mass Spectral Fragmentation Pathways of Phthalate Esters by Gas Chromatography–Tandem Mass Spectrometry. *Anal. Lett.* **2014**, *47* (9), 1579–1588. https://doi.org/10.1080/00032719.2013.879658.

(65) Yinon, J. Mass Spectral Fragmentation Pathways in Phthalate Esters. A Tandem Mass Spectrometric Collision-induced Dissociation Study. *Org. Mass Spectrom.* **1988**, *23* (11), 755–759. https://doi.org/10.1002/oms.1210231104.

(66) Zhang, Q.; Song, J.; Li, X.; Peng, Q.; Yuan, H.; Li, N.; Duan, L.; Ma, J. Concentrations and Distribution of Phthalate Esters in the Seamount Area of the Tropical Western Pacific Ocean. *Mar. Pollut. Bull.* **2019**, *140*, 107–115. https://doi.org/10.1016/j.marpolbul.2019.01.015.

(67) Baloyi, N. D.; Tekere, M.; Maphangwa, K. W.; Masindi, V. Insights Into the Prevalence and Impacts of Phthalate Esters in Aquatic Ecosystems. *Front. Environ. Sci.* **2021**, *9*. https://doi.org/10.3389/fenvs.2021.684190.

(68) Wurl, O.; Ekau, W.; Landing, W. M.; Zappa, C. J. Sea Surface Microlayer in a Changing Ocean – A Perspective. *Elem. Sci. Anthr.* **2017**, *5*, 31. https://doi.org/10.1525/elementa.228.

(69) Zhang, Z.; Cai, W.; Liu, L.; Liu, C.; Chen, F. Direct Determination of Thickness of Sea Surface Microlayer Using a pH Microelectrode at Original Location. *Sci. China Ser. B Chem.* **2003**, *46* (4), 339–351. https://doi.org/10.1360/02yb0192.

(70) Zhengbin, Z.; Liansheng, L.; Zhijian, W.; Jun, L.; Haibing, D. Physicochemical Studies of the Sea Surface Microlayer.

(71) Wurl, O.; Holmes, M. The Gelatinous Nature of the Sea-Surface Microlayer. *Mar. Chem.* **2008**, *110* (1–2), 89–97. https://doi.org/10.1016/j.marchem.2008.02.009.

(72) Chen, Y.; Zhang, N.; Hu, C.; Chen, R.; Yang, G.-P. Controls on the Distribution, Enrichment, and Degradation of Dissolved Organic Matter in the Sea Surface Microlayer of the Yellow Sea and East China Sea. *J. Geophys. Res. Oceans* **2022**, *127* (12), e2022JC019122. https://doi.org/10.1029/2022JC019122.

(73) Mustaffa, N. I. H.; Badewien, T. H.; Ribas-Ribas, M.; Wurl, O. High-Resolution Observations on Enrichment Processes in the Sea-Surface Microlayer. *Sci. Rep.* **2018**, *8* (1), 13122. https://doi.org/10.1038/s41598-018-31465-8.

(74) Engel, A.; Bange, H. W.; Cunliffe, M.; Burrows, S. M.; Friedrichs, G.; Galgani, L.; Herrmann, H.; Hertkorn, N.; Johnson, M.; Liss, P. S.; Quinn, P. K.; Schartau, M.; Soloviev, A.; Stolle, C.; Upstill-Goddard, R. C.; van Pinxteren, M.; Zäncker, B. The Ocean's Vital Skin: Toward an Integrated Understanding of the Sea Surface Microlayer. *Front. Mar. Sci.* **2017**, *4*. https://doi.org/10.3389/fmars.2017.00165.

(75) Del Vento, S.; Dachs, J. Influence of the Surface Microlayer on Atmospheric Deposition of Aerosols and Polycyclic Aromatic Hydrocarbons. *Atmos. Environ.* **2007**, *41* (23), 4920–4930. https://doi.org/10.1016/j.atmosenv.2007.01.062.

(76) Karnatz, J.; Barthelmeß, T.; Sabbaghzadeh, B.; Engel, A. Biochemical Characteristics of the Sea Surface Microlayer in the Central Baltic Sea and Potential Signatures of Cyanobacterial Blooms. *EGUsphere* **2025**, 1–40. https://doi.org/10.5194/egusphere-2025-5385.

(77) Werner, A. C. Vapor Pressures of Phthalate Esters. *Ind. Eng. Chem.* **1952**, *44* (11), 2736–2740. https://doi.org/10.1021/ie50515a063.

(78) Aller, J. Y.; Radway, J. C.; Kilthau, W. P.; Bothe, D. W.; Wilson, T. W.; Vaillancourt, R. D.; Quinn, P. K.; Coffman, D. J.; Murray, B. J.; Knopf, D. A. Size-Resolved Characterization of the Polysaccharidic and Proteinaceous Components of Sea Spray Aerosol. *Atmos. Environ.* **2017**, *154*, 331–347. https://doi.org/10.1016/j.atmosenv.2017.01.053.

(79) Jeilani, Y. A.; Cardelino, B. H.; Ibeanusi, V. M. Density Functional Theory and Mass Spectrometry of Phthalate Fragmentations Mechanisms: Modeling Hyperconjugated Carbocation and Radical Cation Complexes with Neutral Molecules. *J. Am. Soc. Mass Spectrom.* **2011**, *22* (11), s13361-011-0215–0218. https://doi.org/10.1007/s13361-011-0215-8.

(80) Butler, J.; O'Brien, P.; Crain, S.; Scientific, T. F. Determination of DEHP in Culture Media by GC-MS/MS Using PCI Ammonia.

(81) Li, F.; Liu, Y.; Wang, D.; Zhang, C.; Yang, Z.; Lu, S.; Wang, Y. Biodegradation of Di-(2-Ethylhexyl) Phthalate by a Halotolerant Consortium LF. *PLoS ONE* **2018**, *13* (10), e0204324. https://doi.org/10.1371/journal.pone.0204324.

(82) Liang, D.-W.; Zhang, T.; Fang, H. H. P.; He, J. Phthalates Biodegradation in the Environment. *Appl. Microbiol. Biotechnol.* **2008**, *80* (2), 183–198. https://doi.org/10.1007/s00253-008-1548-5.

(83) Xu, X.; Li, T.; Zhen, J.; Jiang, Y.; Nie, X.; Wang, Y.; Yuan, X.-Z.; Mao, H.; Wang, X.; Xue, L.; Chen, J. Characterization of Microplastics in Clouds over Eastern China. *Environ. Sci. Technol. Lett.* **2024**, *11* (1), 16–22. https://doi.org/10.1021/acs.estlett.3c00729.

(84) Ganguly, M.; Ariya, P. A. Ice Nucleation of Model Nanoplastics and Microplastics: A Novel Synthetic Protocol and the Influence of Particle Capping at Diverse Atmospheric Environments. *ACS Earth Space Chem.* **2019**, *3* (9), 1729–1739. https://doi.org/10.1021/acsearthspacechem.9b00132.

(85) Revell, L. E.; Kuma, P.; Le Ru, E. C.; Somerville, W. R. C.; Gaw, S. Direct Radiative Effects of Airborne Microplastics. *Nature* **2021**, *598* (7881), 462–467. https://doi.org/10.1038/s41586-021-03864-x.

(86) Mansuri, A.; Trivedi, C.; Chokshi, S.; Jantrania, K.; Kumar, A. Phthalate Exposure: Prevalence, Health Effects, Regulatory Frameworks, and Remediation. *Chem. Res. Toxicol.* **2025**, *38* (8), 1291–1308. https://doi.org/10.1021/acs.chemrestox.4c00338.

(87) Pietrogrande, M. C.; Rossi, D.; Paganetto, G. Gas Chromatographic–Mass Spectrometric Analysis of Di(2-Ethylhexyl) Phthalate and Its Metabolites in Hepatic Microsomal Incubations. *Anal. Chim. Acta* **2003**, *480* (1), 1–10. https://doi.org/10.1016/S0003-2670(02)01652-5.

(88) Stokes, M. D.; Deane, G.; Collins, D.; Cappa, C.; Bertram, T.; Dommer, A.; Schill, S.; Forestieri, S.; Survilo, M. A Miniature Marine Aerosol Reference Tank (miniMART) as a Compact Breaking Wave Analogue. *Atmospheric Meas. Tech.* **2016**, *9*, 4257–4267. https://doi.org/10.5194/amt-9-4257-2016.

(89) Liu, R.; Tao, Y. Occurrence, Bioaccumulation, and Partitioning of Phthalate Acid Esters in the Third Largest Freshwater Lake (Lake Taihu) in China. *Environ. Res.* **2024**, *263*, 120188. https://doi.org/10.1016/j.envres.2024.120188.

(90) Gao, J.; Chi, J. Biodegradation of Phthalate Acid Esters by Different Marine Microalgal Species. *Mar. Pollut. Bull.* **2015**, *99* (1–2), 70–75. https://doi.org/10.1016/j.marpolbul.2015.07.061.

(91) Kruse, S. M.; Slade, J. H. Heterogeneous and Photosensitized Oxidative Degradation Kinetics of the Plastic Additive Bisphenol-A in Sea Spray Aerosol Mimics. *J. Phys. Chem. A* **2023**, *127* (21), 4724–4733. https://doi.org/10.1021/acs.jpca.3c00127.

(92) Feng, J.-R.; Deng, Q.-X.; Ni, H.-G. Photodegradation of Phthalic Acid Esters under Simulated Sunlight: Mechanism, Kinetics, and Toxicity Change. *Chemosphere* **2022**, *299*, 134475. https://doi.org/10.1016/j.chemosphere.2022.134475.

(93) Tuan Tran, H.; Lin, C.; Bui, X.-T.; Ky Nguyen, M.; Dan Thanh Cao, N.; Mukhtar, H.; Giang Hoang, H.; Varjani, S.; Hao Ngo, H.; Nghiem, L. D. Phthalates in the Environment: Characteristics, Fate and Transport, and Advanced Wastewater Treatment Technologies. *Bioresour. Technol.* **2022**, *344*, 126249. https://doi.org/10.1016/j.biortech.2021.126249.